Neuron

Article

Astrocytes Control Sensory Acuity via Tonic Inhibition in the Thalamus

Graphical Abstract

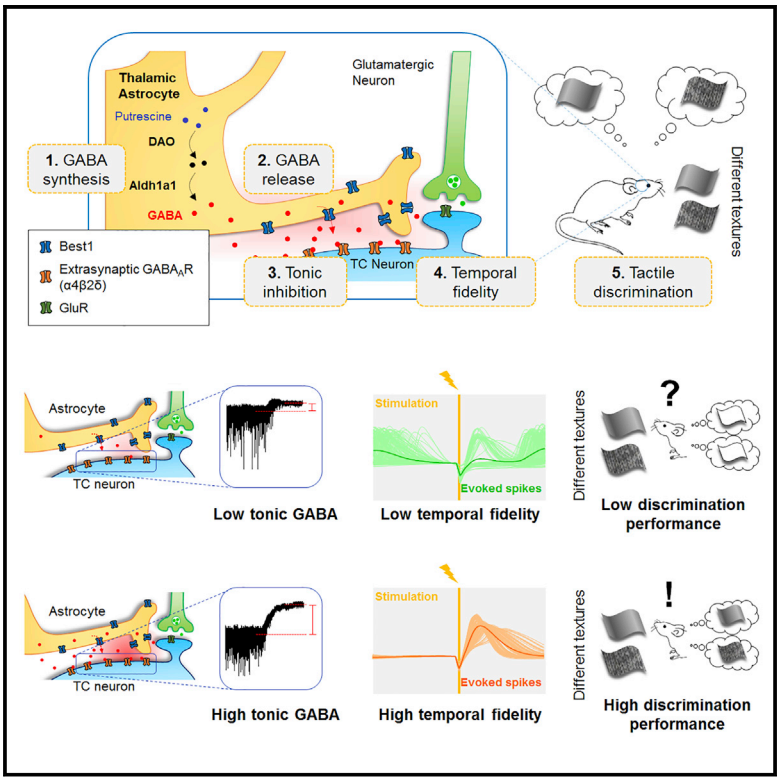

Highlights

- Thalamic astrocytes synthesize GABA via DAO and Aldh1a1 to mediate tonic inhibition
- Tonic GABA improves linearity and temporal fidelity of synaptically evoked TC firing
- Astrocytic tonic GABA improves tactile discrimination performance

Authors

Hankyul Kwak, Wuhyun Koh, Sangwoo Kim, ..., Yong Chul Bae, C. Justin Lee, Eunji Cheong

Correspondence

cjl@ibs.re.kr (C.J.L.), eunjicheong@yonsei.ac.kr (E.C.)

In Brief

Kwak et al. report that astrocytes synthesize GABA using DAO and Aldh1a1 and release GABA through the Best1 channel to mediate tonic GABA in the thalamus. Astrocytic tonic GABA fine-tunes the dynamic range and precision of stimulation to response of TC firing, thus enhancing the performance of sensory discrimination of mice.

Kwak et al., 2020, Neuron *108*, 1–16
November 25, 2020
https://doi.org/10.1016/j.neuron.2020.08.013

CellPress

Please cite this article in press as: Kwak et al., Astrocytes Control Sensory Acuity via Tonic Inhibition in the Thalamus, Neuron (2020), https://doi.org/10.1016/j.neuron.2020.08.013

Neuron

CellPress

Article

Astrocytes Control Sensory Acuity via Tonic Inhibition in the Thalamus

Hankyul Kwak,[1,19] Wuhyun Koh,[2,3,4,19] Sangwoo Kim,[1] Kiyeong Song,[1] Jeong-Im Shin,[2,3] Jung Moo Lee,[3,4,5] Elliot H. Lee,[1] Jin Young Bae,[6] Go Eun Ha,[1] Ju-Eun Oh,[7] Yongmin Mason Park,[2,3,4] Sunpil Kim,[4,5] Jiesi Feng,[8] Seung Eun Lee,[9] Ji Won Choi,[10] Ki Hun Kim,[11] Yoo Sung Kim,[12] Junsung Woo,[3] Dongsu Lee,[1] Taehwang Son,[13] Soon Woo Kwon,[14] Ki Duk Park,[2,10,15] Bo-Eun Yoon,[12] Jaeick Lee,[11] Yulong Li,[8,16,17] Hyunbeom Lee,[7] Yong Chul Bae,[6] C. Justin Lee,[2,3,4,*] and Eunji Cheong[1,18,20,*]

[1]Department of Biotechnology, College of Life Science and Biotechnology, Yonsei University, Seoul 03722, South Korea
[2]Division of Bio-Medical Science &Technology, KIST School, Korea University of Science and Technology, Seoul 02792, South Korea
[3]Center for Glia-Neuron Interaction, Korea Institute of Science and Technology, Seoul 02792, South Korea
[4]Center for Cognition and Sociality, Institute for Basic Science, Daejeon 34126, South Korea
[5]KU-KIST Graduate School of Converging Science and Technology, Korea University, Seoul 02841, South Korea
[6]Department of Anatomy and Neurobiology, School of Dentistry, Kyungpook National University, Daegu 41566, South Korea
[7]Molecular Recognition Research Center, Korea Institute of Science and Technology, Seoul 02792, South Korea
[8]State Key Laboratory of Membrane Biology, Peking University School of Life Sciences, Beijing 100871, China
[9]Virus Facility, Research Animal Resource Center, Korea Institute of Science and Technology, Seoul 02792, South Korea
[10]Convergence Research Center for Diagnosis, Treatment and Care System of Dementia, Korea Institute of Science and Technology, Seoul 02792, South Korea
[11]Doping Control Center, Korea Institute of Science and Technology, Seoul 02792, South Korea
[12]Department of Molecular Biology, College of Natural Science, Dankook University, Cheonan 31116, South Korea
[13]School of Electrical and Electronic Engineering, Yonsei University, Seoul 03722, South Korea
[14]Radiation Medicine Clinical Research Division, Korea Institute of Radiological and Medical Sciences, Seoul, South Korea
[15]KHU-KIST Department of Converging Science and Technology, Kyung Hee University, Seoul 02447, South Korea
[16]Peking-Tsinghua Center for Life Sciences, Academy for Advanced Interdisciplinary Studies, Peking University, Beijing 100871, China
[17]PKU-IDG/McGovern Institute for Brain Research, Beijing 100871, China
[18]POSTECH Biotech Center, POSTECH, Pohang, South Korea
[19]These authors contributed equally
[20]Lead Contact
*Correspondence: cjl@ibs.re.kr (C.J.L.), eunjicheong@yonsei.ac.kr (E.C.)
https://doi.org/10.1016/j.neuron.2020.08.013

SUMMARY

Sensory discrimination is essential for survival. However, how sensory information is finely controlled in the brain is not well defined. Here, we show that astrocytes control tactile acuity via tonic inhibition in the thalamus. Mechanistically, diamine oxidase (DAO) and the subsequent aldehyde dehydrogenase 1a1 (Aldh1a1) convert putrescine into GABA, which is released via Best1. The GABA from astrocytes inhibits synaptically evoked firing at the lemniscal synapses to fine-tune the dynamic range of the stimulation-response relationship, the precision of spike timing, and tactile discrimination. Our findings reveal a novel role of astrocytes in the control of sensory acuity through tonic GABA release.

INTRODUCTION

Sensory information processing is essential for recognition of and response to external stimuli and ultimately for survival. Differentiating sensory stimuli from one another requires fine modulation of various neural circuits, including receptors at the peripheral system and brain structures (McGlone et al., 2014). Thalamus is a sensory gatekeeper in the brain, filtering in and out the sensory information (McCormick and Bal, 1994). In particular, the ventrobasal nucleus (VB) of thalamus delivers tactile information to cortex and is known to be essential for tactile discrimination (Finger, 1972). Recently, the precise spike timing in the ventroposterior medial nucleus (VPm), part of VB, was shown to be a neural code for tactile acuity (Waiblinger et al., 2018). However, how tactile acuity is finely controlled in thalamus remains elusive.

Thalamocortical (TC) neurons in the VB display prominent phasic and tonic γ-aminobutyric acid (GABA) currents (Belelli et al., 2005). Although phasic GABA has been demonstrated to come from GABAergic neurons in the thalamic reticular nucleus (TRN) (Pinault, 2004), the cellular source of tonic GABA in the thalamus is still controversial. Although tonic GABA in VB is affected by the activity of TRN neurons (Herd et al., 2013), a non-neuronal slow GABA source has been reported in the VB

Please cite this article in press as: Kwak et al., Astrocytes Control Sensory Acuity via Tonic Inhibition in the Thalamus, Neuron (2020), https://doi.org/10.1016/j.neuron.2020.08.013

(Jiménez-González et al., 2011). Because of the lack of clear knowledge in molecular and cellular mechanisms, a role of tonic GABA in sensory processing is still unknown.

Previously, astrocytes have been suggested to be the non-neuronal source of tonic GABA in cerebellum, hippocampus, and striatum (Jo et al., 2014; Lee et al., 2010; Yu et al., 2018). The astrocytes synthesize GABA using diverse enzymes, including monoamine oxidase B (MAO-B) (Heo et al., 2020; Park et al., 2019; Yoon et al., 2014) and glutamic acid decarboxylase (GAD) (Wu et al., 2014). Aldehyde dehydrogenase 1a1 (Aldh1a1) has also been shown to synthesize GABA in dopaminergic neurons to mediate phasic GABA (Kim et al., 2015), raising a possibility that other enzymes could be involved in GABA synthesis. However, this possibility has not been examined in thalamic astrocytes.

In this study, we investigated thalamic astrocytes as the source of tonic GABA and its GABA-synthesizing mechanism. Based on the molecular mechanism, we manipulated the tonic GABA current via pharmacological and genetic approaches to understand its function for modulation of TC neurons and control of tactile acuity.

RESULTS

Thalamic Astrocytes as a Source of Tonic GABA

To determine the cellular sources of GABA in the thalamus, we performed whole-cell patch clamp from the VB TC neurons (Figure 1A). We observed both spontaneous phasic and sustained tonic GABA currents, which were blocked by the $GABA_AR$ antagonist gabazine (GBZ) (Figure 1B). The spontaneous inhibitory postsynaptic currents (sIPSC) currents were eliminated by a 2-h pretreatment with concanamycin A (ConA), an inhibitor of the vacuolar H^+ ATPase (Figure 1B), indicating that such currents represent the IPSCs from GABAergic neurons. In contrast, the tonic GABA current was not affected by ConA (Figure 1B), suggesting that the major source of tonic GABA is not from the vesicular release. In regards to a non-vesicular release of GABA, previous studies reported tonic GABA release by the GABA-permeable astrocytic Best1 channel (Lee et al., 2010). Best1 expression was prominent in VB and diminished in Best1 knockout mouse (Best1 KO) (Figures S1A and S1B). Therefore, we tested GABA currents in Best1 KO and found that the tonic GABA current was selectively reduced, regardless of ConA (Figures 1B and 1C) or blockers of ionotropic glutamate receptors (Figures S1C and S1D), whereas the phasic GABA current was not (Figures 1B–1E), suggesting that the source of tonic GABA is non-vesicular and channel mediated. We confirmed that the difference in Best1 KO is not by change in the high-affinity extrasynaptic $GABA_ARs$, as evidenced by no difference in tonic GABA currents induced by 5 μM GABA (Figures 1B and 1C). We performed immunohistochemistry (IHC) and found that Best1 is highly colocalized with GFP-positive pixels in VB of GFAP-GFP mice (Figures 1F and 1G), supporting the tonic GABA release from astrocytes through Best1. To establish astrocyte-specific knockdown (KD) of Best1, we used cre-dependent pSico-Red shBest1 (Jung et al., 2016) and thalamic astrocyte-specific hAldh1l1-cre viruses (Koh et al., 2017) (Figures 1H and S2) and found a significant reduction of tonic GABA. Tonic GABA was significantly reduced by shBest1 (Figures 1I and 1J), indicating that the major portion of tonic GABA is released through astrocytic Best1. In contrast, we did not observe GABA release by a reversal activity of GABA transporters (GATs) (Figures S1E–S1H).

To determine the ultrastructural localization of GABA, immunogold electron microscopic labeling was performed and high GABA content was found in GFP-positive astrocytes (Figure 1K). The gold particle density of astrocytes was about one-tenth of GABAergic terminals (Figure 1L). Based on the ratio and the reported GABA concentration in inhibitory terminals (Fonnum and Walberg, 1973), we estimated the GABA in VB astrocytes to be 4 to ~14 mM, suggesting that astrocyte could be a major source of tonic GABA. To quantify the ambient GABA concentration in VB, we made a dose-response curve of tonic GABA from Best1 KO and estimated the ambient GABA to be ~3.5 μM (Figures S1I and S1J).

Next, we investigated whether thalamic astrocytes can synthesize and release GABA without taking up from other cell types, such as GABAergic neurons. To exclude an external source of GABA, we used cultured primary thalamic astrocytes (Figure S3A). By immunocytochemistry (ICC), we found a substantial amount of GABA without an external source, indicating the existence of a GABA-synthesizing mechanism (Figure S3B). To test whether solitary thalamic astrocytes can release GABA, we performed the sniffer patch using TFLLR, a PAR1 agonist, and GABAc receptor-expressing HEK293T cells (sensor cells), as previously described (Jo et al., 2014) (Figures 1M and S3C–S3G). Application of TFLLR induced a Ca^{2+} signal in the astrocyte and a simultaneous inward current (GABA current) in the sensor cell (Figure 1N). Each GABAc current was normalized to the full-activation current by 100 μM GABA (Figure 1N, inset). The current was abolished by picrotoxin (PTX), indicating that the current was GABAc driven. We found that 68.8% of the thalamic astrocytes were GABA releasing, with an average of 8.41% of full activation (Figure 1O). Using the dose-response curve of GABAc (Yang et al., 2006), the GABA from a single cultured astrocyte could be converted to 0.62 μM (Figure 1O). These results indicate that the thalamic astrocytes have their own GABA-synthesizing mechanism and can release GABA Ca^{2+} dependently.

DAO and Aldh1a1 Synthesize GABA from Putrescine to Mediate Tonic GABA

Given that the solitary thalamic astrocytes can synthesize GABA, we performed IHC to identify GABA-synthesizing enzymes in the thalamus. GAD was absent from both TC neurons and astrocytes (Figures S3H and S3I). Astrocytic MAO-B was reported to synthesize GABA from putrescine to mediate tonic GABA in the cerebellum (Yoon et al., 2014) (Figure 2A). Although we found a high level of putrescine in both astrocytes and neurons (Figures 2B and 2C), MAO-B was minimally expressed in both astrocytes and neurons (Figures 2B and 2C), raising the possibility that other putrescine degradation enzymes might be involved. As an alternative to the MAO-B pathway, diamine oxidase (DAO) in the gastric mucosa (Hougaard et al., 1992) and subsequent Aldh1a1 in the striatum (Kim et al., 2015) are reported to catalyze the conversion of putrescine into GABA. We found that DAO is

Please cite this article in press as: Kwak et al., Astrocytes Control Sensory Acuity via Tonic Inhibition in the Thalamus, Neuron (2020), https://doi.org/10.1016/j.neuron.2020.08.013

CellPress

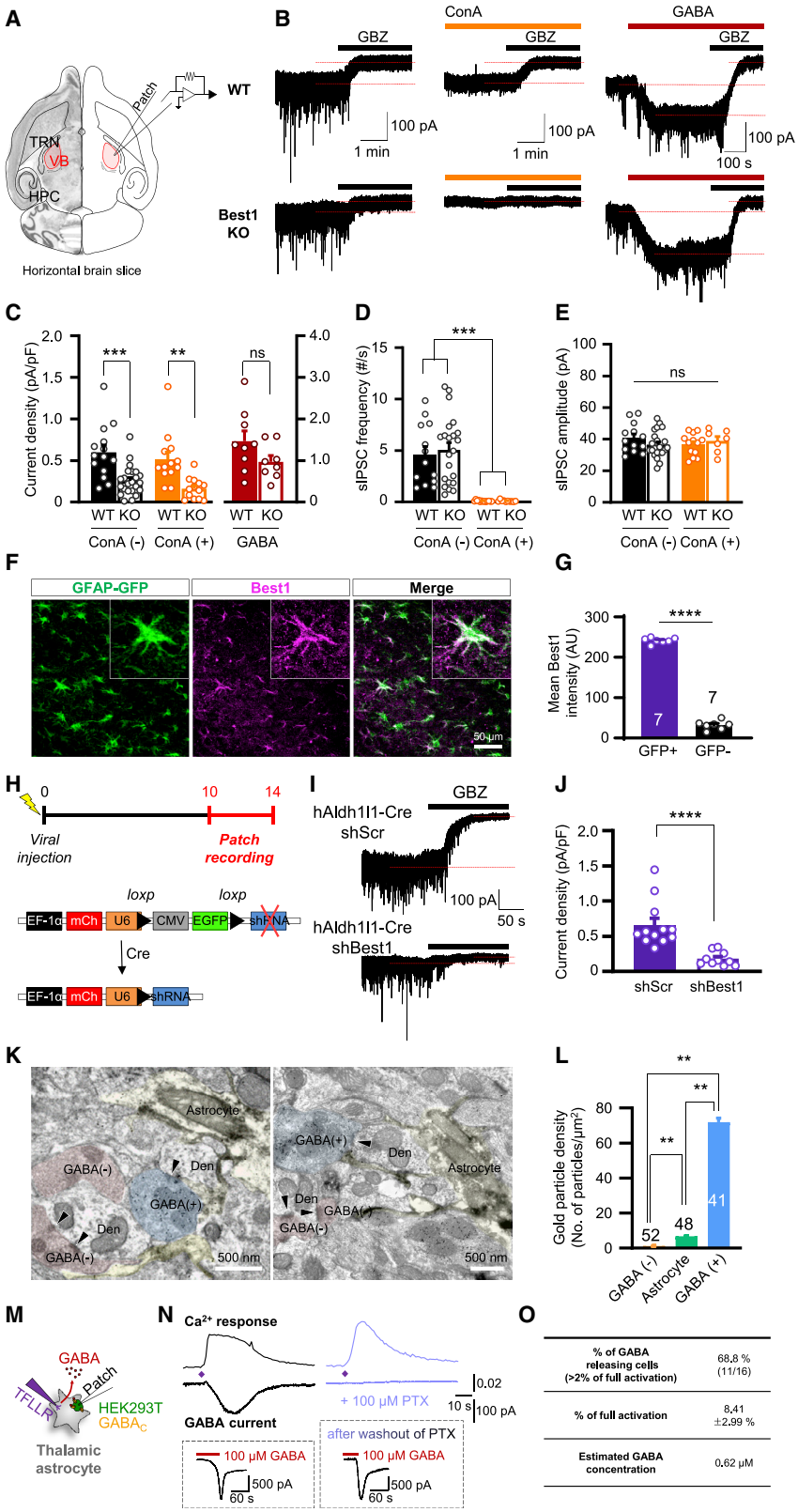

Figure 1. Tonic GABA Originates from Non-neuronal Sources

(A) Scheme of the whole-cell patch clamp in the VB thalamus.

(B) Traces of phasic and tonic GABA currents from wild-type (WT) and Best1 KO, with or without ConA or GABA.

(C–E) Bar graph of tonic GABA currents (C) and sIPSC frequency (D) and amplitude (E) from each group.

(F and G) Images (F) and bar graph (G) of Best1 staining in GFAP-GFP mice. Numbers and individual dots indicate slices.

(H) Timeline (top) and scheme (bottom) of Cre-dependent gene silencing. See also Figure S2.

(I and J) Traces (I) and bar graph (J) of tonic GABA currents in shScr or shBest1.

(K) Immunogold labeling of GABA in GFAP-GFP mice. Arrowheads indicate synapses. GABA(−), GABA-negative terminal; GABA(+), GABA-positive terminal; Den, dendrite.

(L) Bar graph of gold particle density.

(M) Scheme of the sniffer patch. See also Figures S3A and S3B.

(N) Left: representative Ca^{2+} response from the thalamic astrocyte and GABAc current from the sensor cell. Right (blue): responses with PTX application. Inset: full activation of GABAc. See also Figures S3C–S3G.

(O) Table of solitary astrocyte-mediated GABA responses.

Data are presented as mean ± SEM. Numbers and individual dots refer to cells unless otherwise clarified. *p < 0.05; **p < 0.01; ***p < 0.001; ****p < 0.0001; Sidak's multiple comparisons test (C-E), Student's t test (G-J), and Kruskal-Wallis test (L).

Please cite this article in press as: Kwak et al., Astrocytes Control Sensory Acuity via Tonic Inhibition in the Thalamus, Neuron (2020), https://doi.org/10.1016/j.neuron.2020.08.013

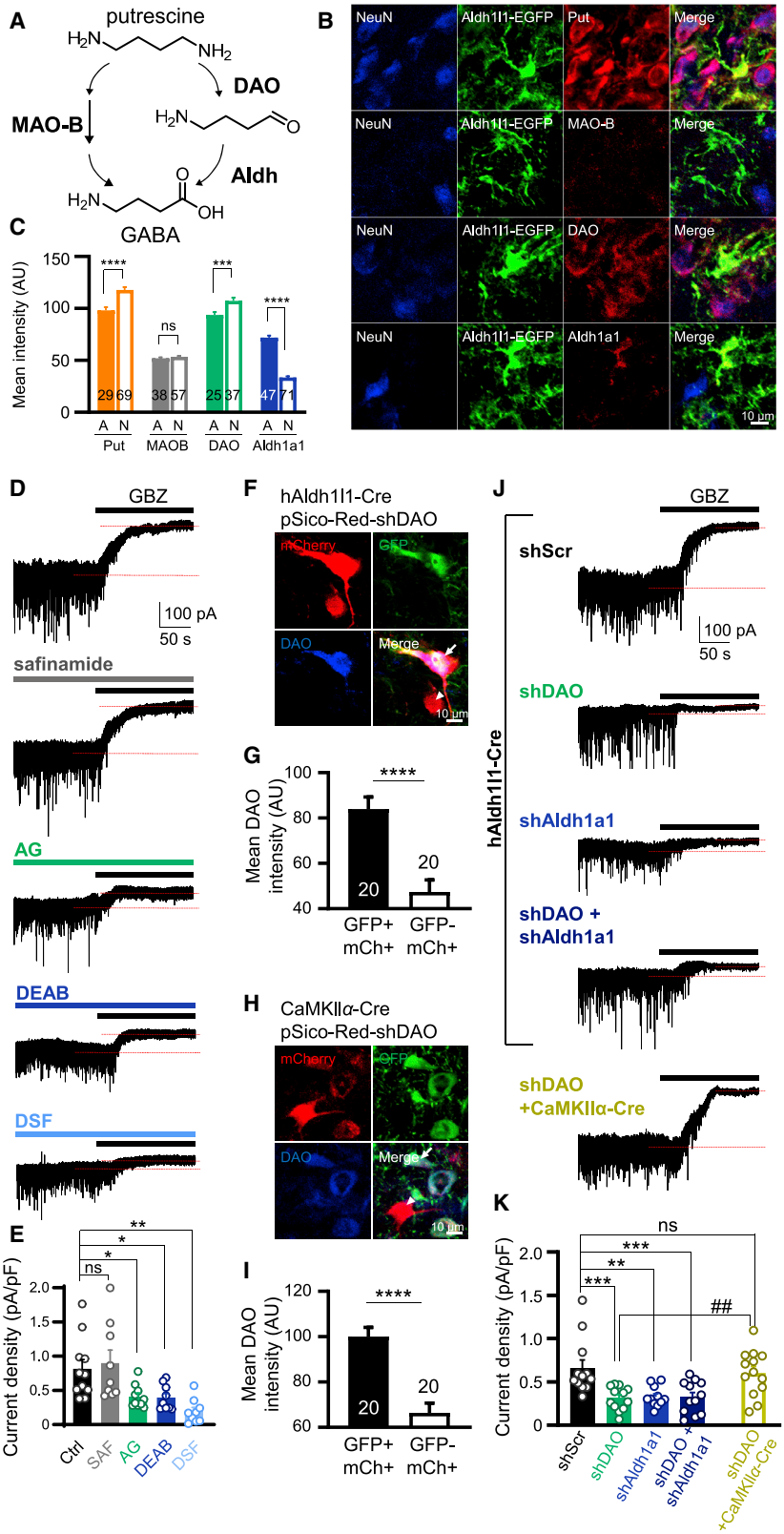

Figure 2. DAO and Aldh1a1 Synthesize GABA from Putrescine to Mediate Tonic GABA

(A) Putrescine to GABA pathways.

(B and C) Images (B) and bar graph (C) of GABA-synthesizing enzymes from Aldh1l1-EGFP mice. The mean red intensity is measured within either the Aldh1l1-EGFP-positive (indicated as A) or the NeuN-positive (indicated as N) area. Put, putrescine.

(D and E) Traces (D) and bar graph (E) of tonic GABA currents with pharmacological inhibition.

(F–I) Immunostaining (F and H) and quantification (G and I) of DAO within Cre-negative and Cre-positive cells infected with pSico-Red-shDAO. Arrows, Cre-negative (GFP+/mCh+) cells; arrowheads, Cre-positive (GFP−/mCh+) cells. See also Figure S2.

(J and K) Traces (J) and bar graph (K) of tonic GABA currents under various combinations of Cre/shRNA viruses.

Data are presented as mean ± SEM. Numbers and individual dots refer to cells. *p < 0.05; **p < 0.01; ***p < 0.001; Student's t test (C, G, and I) and ordinary one-way ANOVA (E and K). ##p < 0.01; Student's t test (K).

Please cite this article in press as: Kwak et al., Astrocytes Control Sensory Acuity via Tonic Inhibition in the Thalamus, Neuron (2020), https://doi.org/10.1016/j.neuron.2020.08.013

expressed in both astrocytes and neurons in the VB (Figures 2B and 2C), whereas Aldh1a1 was only expressed in astrocytes, which suggests that DAO and Aldh1a1 could be the GABA-synthesizing enzymes in astrocytes.

We next tested the effect of specific inhibitors (Figures S3J–S3M) of each candidate enzyme on the tonic GABA current. Inhibition of DAO by aminoguanidine (AG) had a significant blocking effect on tonic GABA, whereas MAO-B inhibitor safinamide had no effect (Figures 2D and 2E). To determine whether Aldh1a1 is involved, we used N,N-diethylaminobenzaldehyde (DEAB), an inhibitor of Aldh1a1, but not of Aldh1l1 (Morgan et al., 2015). Tonic GABA was reduced by 10 μM DEAB, suggesting that Aldh1a1 is the major GABA-synthesizing enzyme. We also found a significant reduction in tonic GABA by 1 μM disulfiram (DSF), a broad inhibitor of Aldh. Furthermore, astrocyte-specific (hAldh1l1-Cre) gene silencing of either DAO or Aldh1a1 resulted in a lower level of the tonic GABA, whereas neuron-specific (Ca^{2+}/calmodulin-dependent protein kinase IIα [CaMKIIα]-Cre) gene silencing did not (Figures 2F–2K and S2). DAO and Aldh1a1 synthesize GABA via a single pathway, as evidenced by the lack of synergistic decrease of tonic GABA by astrocytic gene silencing of both DAO and Aldh1a1 (Figures 2J and 2K). These results indicate that astrocytic DAO and Aldh1a1 are the major GABA-synthesizing enzymes in thalamic astrocytes.

Real-Time Assessment of GABA Reveals that a Single Astrocyte Uses DAO, Aldh1a1, and Best1 to Synthesize and Release GABA

To confirm the mechanisms of GABA synthesis and release from an individual thalamic astrocyte in an isolated system, we used short hairpin RNAs (shRNAs) in the primary thalamic astrocyte (Figures 3A and 3B). Consistent with the *ex vivo* results (Figure 2), the TFLLR-induced GABA current was eliminated by shDAO, shAldh1a1, and shBest1, but not by shMAO-B (Figures 3C–3E). Furthermore, GABA synthesis by DAO and Aldh1a1 was confirmed by ICC with an antibody against GABA (Figures 3F–3H and S4A–S4C). Altogether, these results provide direct evidence of GABA synthesis in a single thalamic astrocyte through the DAO and Aldh1a1 pathway.

Metabolic Diversity as a Consequence of Enzymatic Diversity

Utilization of DAO to synthesize GABA is profoundly different from astrocytes in other regions (Figure S4D). To investigate the metabolic consequence of the different GABA-synthesizing enzymes, we analyzed GABA-related metabolites of the cultured astrocytes from the thalamus, cerebellum, and hippocampus. The region-specific astrocytes were differentiated by principal-component analysis (PCA) and heatmap analysis (Figures 3I and 3J). The levels of putrescine and GABA were higher in both thalamic and cerebellar astrocytes compared with hippocampal astrocytes (Figures 3K and 3L), consistent with a previous report of the lack of GABA synthesis in hippocampal astrocytes under a physiological condition (Jo et al., 2014). Although cerebellar astrocytes showed a high level of N-acetyl-GABA, an intermediate metabolite in the MAO-B pathway, thalamic astrocytes presented a lower level of N-acetyl-GABA than did cerebellar astrocytes (Figures 3K and 3L). These results underscore the regional diversity of astrocytes by demonstrating that thalamic astrocytes use the DAO pathway, rather than MAO-B, to produce GABA.

Acutely Isolated Adult Astrocytes Synthesize GABA via DAO

To estimate the contribution of the DAO pathway in GABA synthesis under more a *in vivo*-like condition, we performed sniffer-patch recordings from a single acutely dissociated VB astrocyte. To visually identify the VB astrocytes, we used Aldh1l1-CreERT2 crossed with RCL-tdTomato mice (Figures S4E and S4F). VB astrocytes were mechanically dissociated and subjected to the sniffer patch (Figure 3M). Upon TFLLR application, GABA release was observed in 75% of the astrocytes, with 1.384% of the full activation current (Figures 3N and 3O), which could be converted to 0.27 μM GABA from one astrocyte (Figure 3P). The GABA current was significantly reduced by AG (Figures 3N–3P), indicating that DAO is required for GABA production. These results imply that astrocytic DAO serves as the major source of tonic GABA in the adult thalamus *in vivo*.

Various Ways to Enhance Tonic GABA Current

So far, by delineating the mechanisms of GABA synthesis and release in astrocytes, we found genetic and pharmacological tools to reduce the tonic GABA current without affecting the phasic GABA. We next explored various ways to enhance tonic GABA in VB. It was reported that norepinephrine (NE) reduces spontaneous firing of VB neurons. More importantly, astrocytes in various regions express adrenergic receptors (ARs) to mediate Ca^{2+} transients by NE input (Ding et al., 2013) and inhibit adjacent neurons (Bar El et al., 2018). Thus, we hypothesized that activation of the astrocytic AR might dynamically enhance the tonic GABA. First, we used a recently developed NE sensor, $GRAB_{NE2m}$ (Feng et al., 2019) (Figures 4A and 4B), to investigate whether the thalamus-projecting adrenergic locus coeruleus (LC) fibers (Schwarz and Luo, 2015) can release NE onto astrocytes. We found that local stimulation of VB caused a release of NE onto astrocytes in a frequency-dependent manner (Figures 4C and 4D), raising the possibility that thalamic astrocytes can dynamically respond to NE. Consistently, we found Ca^{2+} elevation in VB astrocytes by NE infusion in brain slices of mouse co-injected with AAV-hAldh1l1-Cre and AAV-FLEX-jRCaMP1a (a red Ca^{2+} sensor) viruses (Figures 4E and 4F). More importantly, NE application significantly increased the tonic GABA current (Figures 4G and 4H), which was absent from Best1 KO, mainly via the α1 AR-phospholipase C (PLC) pathway (Figures S5A–S5F). These results suggest that NE input onto VB astrocytes enhances tonic GABA via Ca^{2+}-dependent GABA release through Best1. In addition to an astrocytic effect, NE showed a direct effect on TC neurons to increase membrane excitability (Figures S5G–S5L). This neuronal effect by NE could be a potential confounding factor when an astrocyte-specific effect is desired.

The second way to enhance tonic GABA was to use an optogenetic tool, optoSTIM1 (Kyung et al., 2015), that upon blue-light stimulation opens the endogenous Orai channel to allow Ca^{2+} influx (Figure 4I). We found that astrocyte-specific activation of

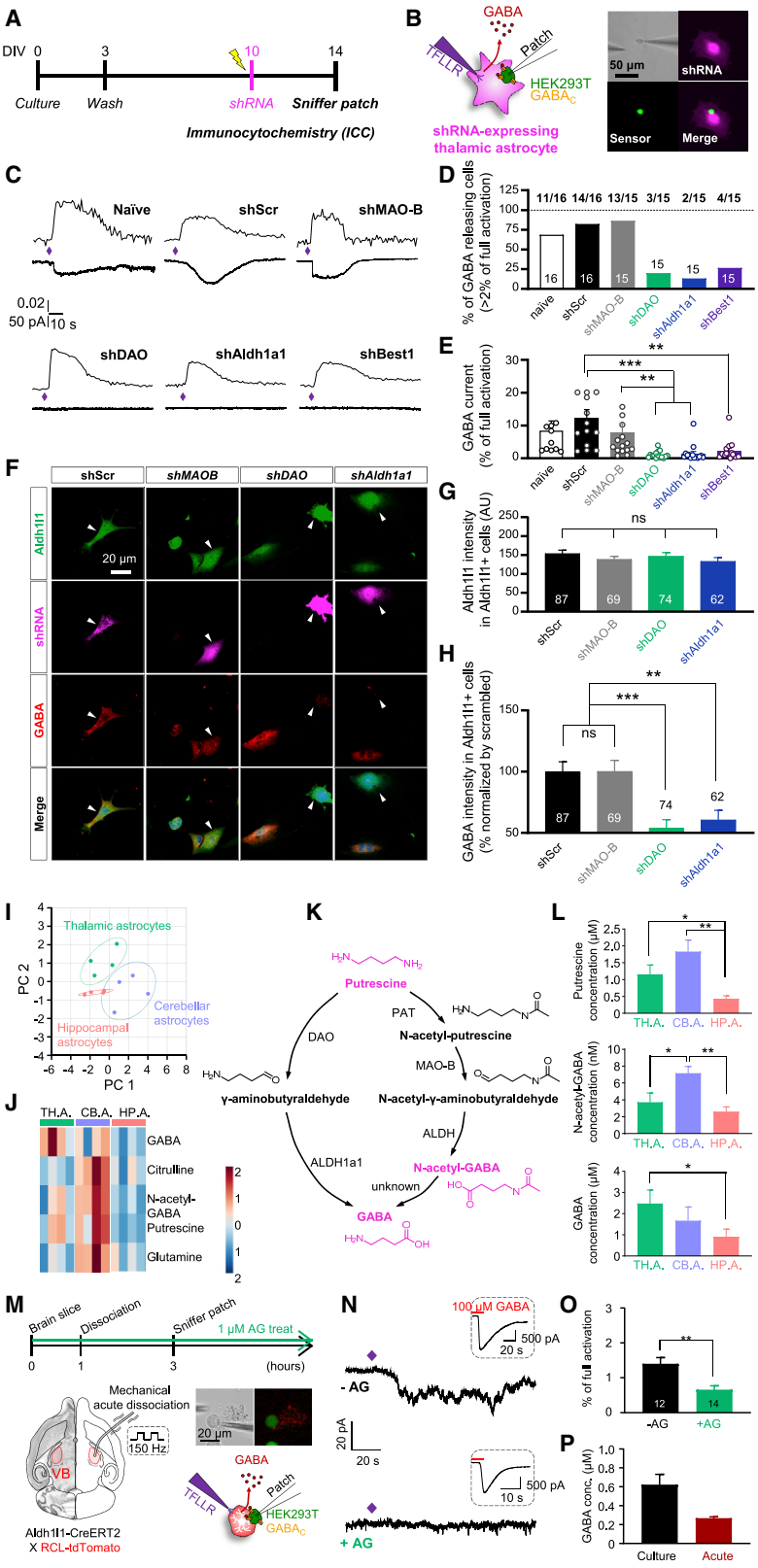

Figure 3. Unique GABA-Synthesizing Pathway and Its Metabolic Consequences

(A and B) Timeline (A) and scheme (B) of the sniffer patch using the shRNA-expressing astrocyte (pink) and the sensor cell (green).

(C) Traces of simultaneous Ca^{2+} response in astrocytes and GABAc currents in sensor cells.

(D and E) Percentage of GABA-releasing astrocytes (D) and GABA current (E) in each condition.

(F) Images of GABA with gene silencing of each candidate enzyme. Arrow, transfected astrocyte.

(G and H) Mean intensities of Aldh1l1 (G) and GABA (H) in transfected cells from each condition. GABA intensity was normalized to the controls.

(I and J) PCA (I) and heatmap (J) of GABA-related metabolites from thalamic (TH.A, green), cerebellar (CB.A, blue), and hippocampal (HP.A, red) astrocytes. Dots refer to batch number.

(K) Metabolites in putrescine degradation pathways. Quantified metabolites are highlighted in pink.

(L) Bar graphs for concentrations of each metabolite from each brain region.

(M) Timeline and scheme of the sniffer patch using acutely dissociated VB astrocytes. See also Figure S4.

(N and O) Traces (N) and percentage of full activation (O) of GABAc currents with AG (+AG) or without AG (−AG). Inset: full activation currents.

(P) GABA concentration based on the dose-response curve. Data are presented as mean ± SEM. Numbers and individual dots refer to cells unless otherwise clarified. *$p < 0.05$; **$p < 0.01$; ***$p < 0.001$; Kruskal-Wallis test (E, G, and H) and Student's t test (L and O)

Please cite this article in press as: Kwak et al., Astrocytes Control Sensory Acuity via Tonic Inhibition in the Thalamus, Neuron (2020), https://doi.org/10.1016/j.neuron.2020.08.013

CellPress

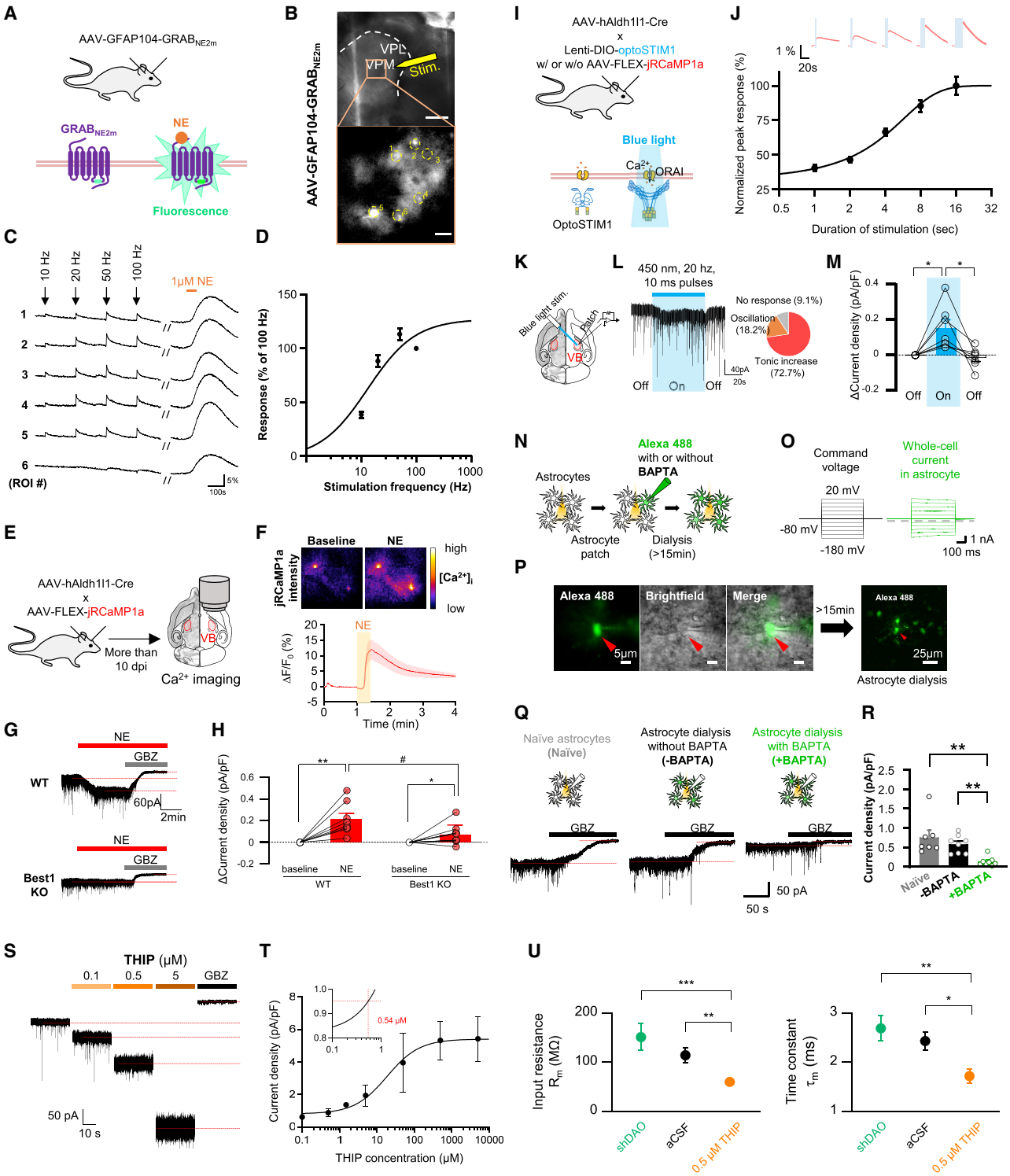

Figure 4. Various Ways to Modulate the Tonic GABA Current

(A) Scheme of GRAB$_{NE2m}$ working.

(B) Location of stimulation (top) and GRAB$_{NE2m}$ expression (bottom). Circles, ROIs, Scale bar: top, 200 μm; bottom, 20 μm.

(C) Responses of GRAB$_{NE2m}$ by electrical stimuli (10, 20, 50, and 100 Hz) and NE (1 μM) application.

(D) Peak amplitude curve (normalized by peak amplitude from 100 Hz stimulation).

(E and F) Scheme (E) and quantification (F) of Ca^{2+} responses in astrocytes using jRCaMP1a. (F) Representative Ca^{2+} response and mean Ca^{2+} transient.

(legend continued on next page)

Please cite this article in press as: Kwak et al., Astrocytes Control Sensory Acuity via Tonic Inhibition in the Thalamus, Neuron (2020), https://doi.org/10.1016/j.neuron.2020.08.013

Orai induced the Ca^{2+} signal in astrocytes (Figure 4J) and tonic GABA increase in most (~73%) TC neurons (Figures 4K–4M), whereas a minor portion showed oscillation (~18%) or no response (~9%) (Figure 4L, right). We found that the opto-STIM1-induced current was about 0.15 pA/pF (Figure 4M), similar to the NE-induced current (Figure 4H). Therefore, opto-STIM1 is an effective way to enhance the tonic GABA current. The necessity of Ca^{2+} signaling in astrocyte for GABA release was further investigated. Intracellular Ca^{2+} chelator, BAPTA, and Alexa Fluor 488 were loaded via patch pipette and dialyzed (>15 min) to nearby astrocytes through the gap junction (Serrano et al., 2006) (Figures 4N–4P). The cellular identity was confirmed by passive conductance (Figure 4O). We found that the tonic GABA current was significantly decreased by BAPTA, indicating that Ca^{2+} is necessary for tonic GABA release from astrocytes (Figures 4Q and 4R). However, considering that astrocytes can release various gliotransmitters upon Ca^{2+} increase (Woo et al., 2012), it might be difficult to isolate the effect of astrocytic GABA.

The third way to enhance the tonic GABA current was to use THIP (4,5,6,7-tetrahydroisoxazolo[5,4-c]pyridin-3-ol), an agonist for δ-$GABA_A$R. We measured THIP-induced tonic GABA currents and obtained a dose-response curve (Figures 4S and 4T). Using the curve, we calculated the concentration of THIP that induces the similar level of tonic GABA current by astrocytic Ca^{2+} activation (~0.95 pA/pF = 0.8 + 0.15 pA/pF) and found it to be about 0.5 μM (Figure 4T, inset). From these explorations, we suggest that THIP can be a useful way to directly enhance the tonic GABA current in VB TC neurons without confounding effects.

Tonic GABA Fine-Tunes the Dynamic Range of Stimulation-Response and Precision of Spike Timing of TC Neurons

Inspired by the various tools to control the tonic GABA, we next examined the function of tonic GABA. First, we found that the tonic GABA reduces both the membrane resistance (R_m) and the time constant (τ_m = RC) (Figure 4U). To confirm the inhibitory effect of tonic GABA on synaptically elicited firing, we measured the spike probability evoked by ten stimuli (0.1 ms duration) at varying intensities (50 to ~1,000 μA) applied to medial lemniscus afferent (Figure 5A), the input structure from the somatosensory system (Castro-Alamancos, 2002). The spike probability was significantly increased by the decrease of tonic GABA (GBZ, AG, DSF, or Best1 KO) (Figures 5B–5D). In contrast, the spike probability was reduced by THIP, whereas safinamide had no effect. The increase of spike probability by decreasing tonic GABA was of astrocyte origin, as evidenced by the enhanced spike probability after astrocyte-specific KD of DAO, Aldh1a1, or Best1 (Figures 5E–5H). The inhibitory effect was shown as a negative correlation (R = −0.939) between tonic GABA and spike probability (Figure 5I).

VB TC neurons transfer high-frequency information (>100 Hz) during sensory stimulation (Deschênes et al., 2003; Urbain et al., 2015). To determine the role of tonic GABA in high-frequency input processing, we measured the synaptically evoked spikes induced by 100 Hz stimulation (10 stimuli) at varying intensities (S1 = 200, S2 = 400, S3 = 600, S4 = 800, S5 = 1,000, and S6 = 1,500 μA) (Figure 5J). In a low-tonic GABA condition (shDAO), abnormally saturated spike generation was observed even at low intensity (400 μA) compared with the control (aCSF) (Figure 5J). In contrast, in a high-tonic GABA condition (0.5 μM THIP), a gradual increase in spike generation was observed, corresponding to the increased stimulation intensities (Figure 5J). The stimulation-response curve indicates an enhanced dynamic range and linearity in high-tonic GABA (THIP) responding to a range of stimuli intensities at the lemniscal synapse (Figure 5K).

Linearity of the stimulus-response curve is reported to improve reconstruction of sensory input (Sherman, 2001) and discriminability (Wang et al., 2010). Given that tonic GABA increases the dynamic range and linearity of the stimulus-to-response relationship, we adopted computational modeling (Wang et al., 2010) (see also STAR Methods). Based on the algorithm to infer the original stimulus when various stimuli (S1 to S6) were given, we simulated discrimination matrices (Figure 5L). The diagonal factors in the matrices indicate the probability of correct discrimination (Figure 5L). We found that the high-tonic GABA (THIP) shows a higher probability of correct discrimination throughout all stimuli, whereas shDAO shows a low probability of correct discrimination among S3 to S6 (Figure 5L). We calculated the overall discrimination performance (sum of the diagonal factors) and found that tonic GABA improves discrimination performance (Figure 5M).

To analyze synaptic coupling, we generated raster plots of individual spikes (black dots) and average frequency histograms (Figure 5N). Low-tonic GABA (shDAO) showed scattered spike timing with a noisy frequency histogram (Figure 5N) and with prominent extra spike generation after the 10^{th} stimulus has been completed (Figure 5N). In contrast, the THIP condition showed high precision and noise-free spike generation in response to each stimulus (Figure 5N). Quantitatively, high-tonic

(G and H) Traces (G) and bar graphs (H) of NE-evoked tonic GABA currents.
(I) Scheme of optoSTIM1 working.
(J) Ca^{2+} response induced by varying durations of stimulation and the quantified stimulation-response curve.
(K) Scheme of patch clamp during blue-light stimulation.
(L) Trace of tonic GABA increase by 1 min light stimulation and a pie chart of response types.
(M) Bar graph of light-evoked tonic GABA currents.
(N) Scheme of BAPTA-mediated Ca^{2+} chelating.
(O) Passive conductance of astrocyte.
(P) Images of astrocytic dialysis through astrocytic syncytium.
(Q and R) Traces (Q) and bar graph (R) of tonic GABA current from naive, BAPTA negative (−BAPTA), and BAPTA positive (+BAPTA).
(S and T) Trace (S) and response curve (T) of tonic current evoked by THIP. Inset: THIP concentration evoking a 0.15 pA/pF increase in tonic current.
(U) Bar graphs of membrane input resistance and time constant.
Data are presented as mean ± SEM. Individual dots refer to cells. *p < 0.05; **p < 0.01; ***p < 0.001; Wilcoxon test (M), Kruskal-Wallis test (R and U) and paired t test (H). #p < 0.05; unpaired t test (H).

Please cite this article in press as: Kwak et al., Astrocytes Control Sensory Acuity via Tonic Inhibition in the Thalamus, Neuron (2020), https://doi.org/10.1016/j.neuron.2020.08.013

CellPress

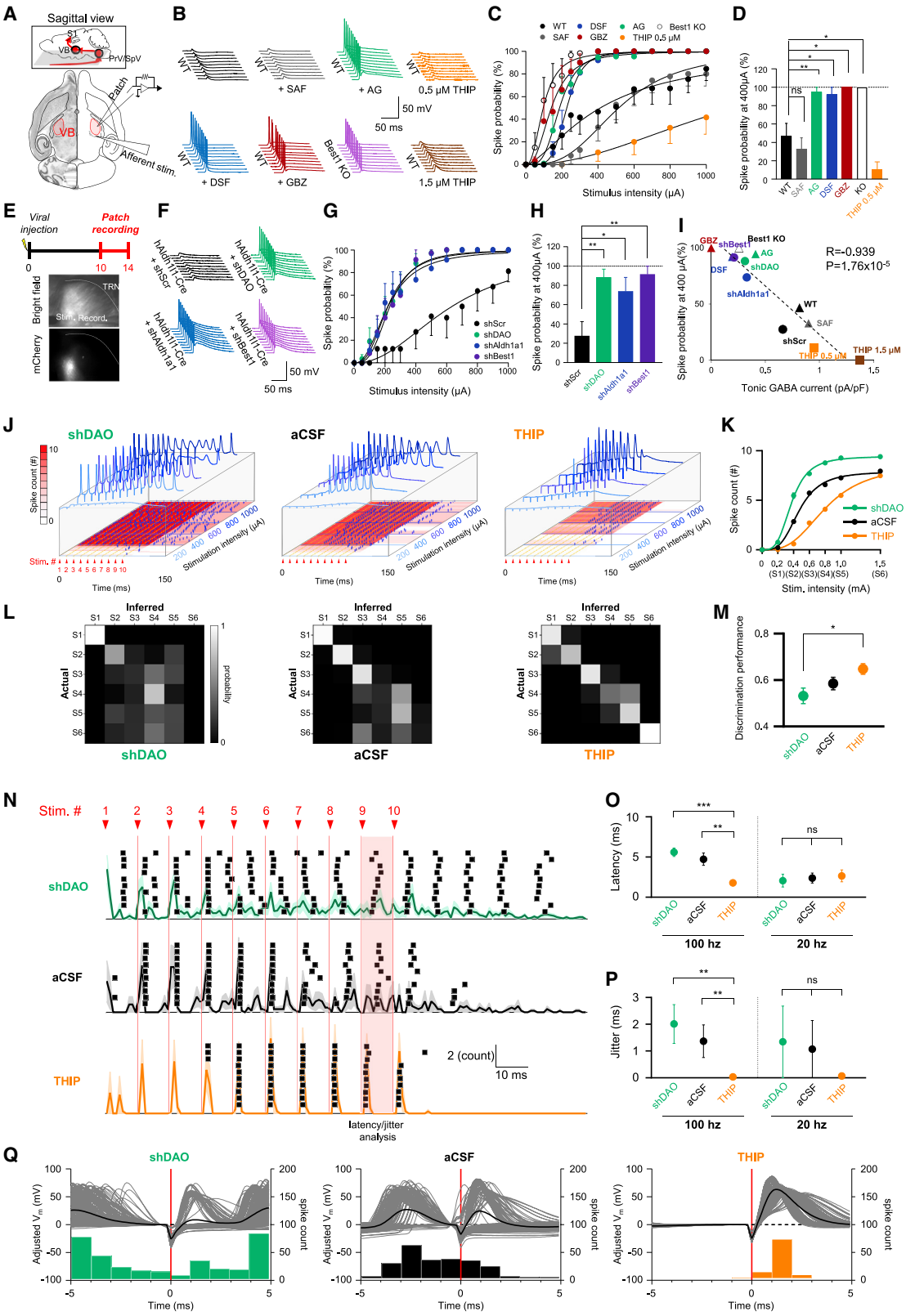

(legend on next page)

Please cite this article in press as: Kwak et al., Astrocytes Control Sensory Acuity via Tonic Inhibition in the Thalamus, Neuron (2020), https://doi.org/10.1016/j.neuron.2020.08.013

GABA (THIP) enhanced the temporal fidelity of synaptically induced spike generation at 100 Hz with significantly shorter latency (Figure 5O) and spike jitter (Figure 5P). Furthermore, the time-locked peri-stimulus traces and frequency histograms of spike time recapitulated that lower-tonic GABA showed spurious spike generation, whereas high-tonic GABA showed no spurious spike (Figure 5Q). In addition, the population synchrony was decreased by the tonic GABA current (Figures S6B–S6E), consistent with a previous report that tonic GABA reduces synchrony (Maex and De Schutter, 1998). The effect of tonic GABA on temporal fidelity was not significant at a lower frequency range (20 Hz) (Figures 5O and 5P). The lemniscal excitatory postsynaptic potential (EPSP) is reported to have fast kinetics (Kao and Coulter, 1997). Upon increasing the stimulation interval (50 ms), the EPSP by each stimulus appears to have sufficient time to fully decay to recover to the baseline potential before the next stimulus, independent of the tonic GABA level.

These changes in the stimulus-response relationship likely result from changes in the postsynaptic neuron's input resistance (R_m), which proportionally influences the time constant ($\tau_m = RC$) (Figure 4U), rather than presynaptic mechanisms (Figures S7A and S7B), as evidenced by a decrease in the time course of synaptic integration and after depolarization upon the increase in tonic GABA (Figures S7C–S7F).

Tonic GABA Improves Temporal Resolution of TC Neurons

It has been reported that sensory input convergence occurs in the thalamus. When two independent inputs converge onto a single TC neuron, two inputs should be distinguished for better discrimination of information. We hypothesized that low-tonic GABA would cause a broad response time window by slow EPSP kinetics (higher τ_m), which would lead to an overlap of response windows if another input arrives with a short time interval and disables the TC neuron from distinguishing two inputs. In contrast, high-tonic GABA should narrow response time window by lower τ_m, enhancing the temporal discrimination between the two inputs.

To test this hypothesis, we used two fine theta glasses, located to activate two independent lemniscal fibers (Figures 6A and 6B). Independence of the two inputs was verified by linear excitatory postsynaptic current (EPSC) summation (Figure 6C) and no heterosynaptic depression (Figures 6D and 6E) by simultaneous and paired-pulse stimulation of the two inputs, respectively. When two inputs were verified to be independent, we measured the probability of successful generation of spikes by stimuli pairs with various inter-stimulus intervals (ISIs). We found that the neurons of high-tonic GABA (THIP) successfully generate spike pairs even with short ISI (3 ms), whereas shDAO could not do so until ISI reaches 7 ms (Figures 6F and 6G). We defined the temporal resolution as the inverse value of minimum ISI, in which the postsynaptic TC neuron can discriminate the two inputs (i.e., successful generation of spike pairs). We found that tonic GABA improves temporal resolution so that a single TC neuron receiving two inputs can discriminate each input by successfully generating spikes (Figure 6H).

Tonic GABA from Astrocyte Improves Tactile Discrimination

Given that tonic GABA enhances spike discrimination (Figure 5L) and temporal resolution (Figure 6) *ex vivo*, we next investigated the *in vivo* function of tonic GABA in sensory processing through VB. We performed the tactile-based novel object recognition test (tNORT), similar to a previous study (Wu et al., 2013) (Figure 7A). The relative exploring time (discrimination index [DI]) was measured iteratively replacing the texture and gradually increasing the textual difference (ΔG) (Figure 7A). We found that astrocytic KD of Best1, DAO, or Aldh1a1 showed a significantly lower DI in test A compared with shScr (Figure 7C). In contrast, there was no significant difference in DI during test B (Figure 7C). These results imply that in lower-tonic GABA, mice could not discriminate the small differences in texture (ΔG = 180) but could still recognize the larger difference (ΔG = 320). We confirmed that the changes in DI did not result from changes in locomotion (Figure 7B) or short-term memory (Figure 7D) by open-field test (OFT) or standard NORT, respectively.

To test the effect of enhancement of tonic GABA, we performed tNORT 30 min after a bilateral THIP infusion via cannulas targeting VB (Figures 7E and 7F). The concentration, volume, and speed (30 μM, 0.2 μL, and 0.1 μL/min) were calculated so that THIP reached a local concentration of 0.2 to ~0.5 μM in VB during the behavioral task to mimic the level of tonic GABA released from activated astrocytes (Figure 5). THIP infusion did

Figure 5. Tonic GABA Regulates the Synaptically Evoked Spike

(A) Scheme of recording the lemniscus-evoked spike.
(B) Traces of spikes by 400 μA stimulation.
(C and D) Spike probability by various intensities (C) and 400 μA intensity (D) from each group.
(E) Timeline of virus injection (top) and images of stimulation and recording sites (bottom).
(F) Traces of spikes by 400 μA stimulation with astrocytic gene silencing.
(G and H) Spike probability by various intensities (G) and 400 μA intensity (H) from each group.
(I) Correlation between tonic GABA current and spike probability at 400 μA.
(J) Spikes evoked by 100 Hz stimuli with varying intensities. Blue dots shows the peak time of spikes. The color map indicates the total number of spikes by each 10-stimuli train.
(K) Stimulation-to-response curve of spikes generated by ten stimuli.
(L) Discrimination performance matrices.
(M) Bar graph of discrimination performance.
(N) Raster plots and time histogram of spikes (1 ms bin).
(O and P) Spike latencies (O) and jitters (P) calculated at the 9th to 10th stimulation section (shaded by red).
(Q) Representative all-spike-evoked traces and corresponding histogram are superimposed to show a peri-stimulus-time histogram (PSTH).
Data are presented as mean ± SEM. *p < 0.05; **p < 0.01; ***p < 0.001; Kruskal-Wallis test (D, H, O, and P) and Student's t test (M).

Please cite this article in press as: Kwak et al., Astrocytes Control Sensory Acuity via Tonic Inhibition in the Thalamus, Neuron (2020), https://doi.org/10.1016/j.neuron.2020.08.013

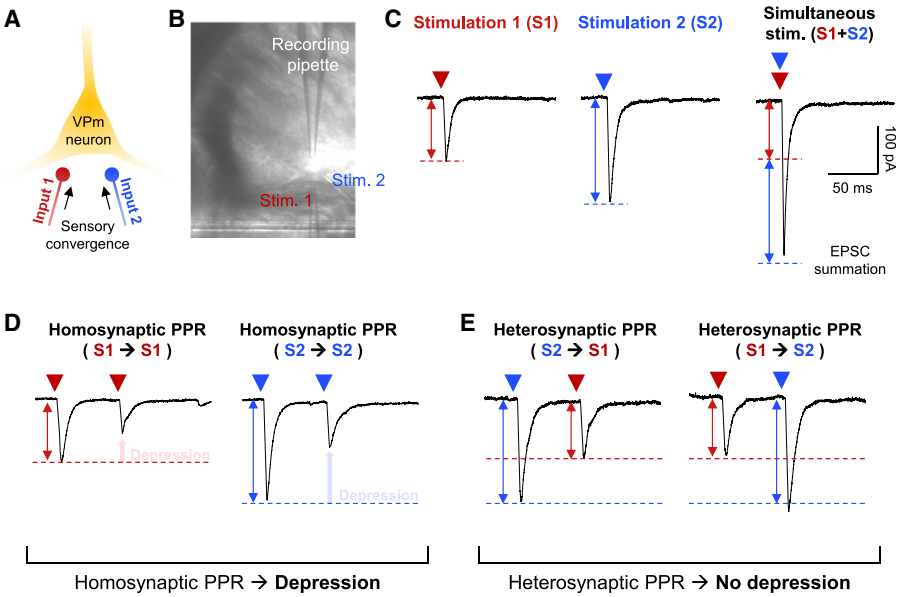

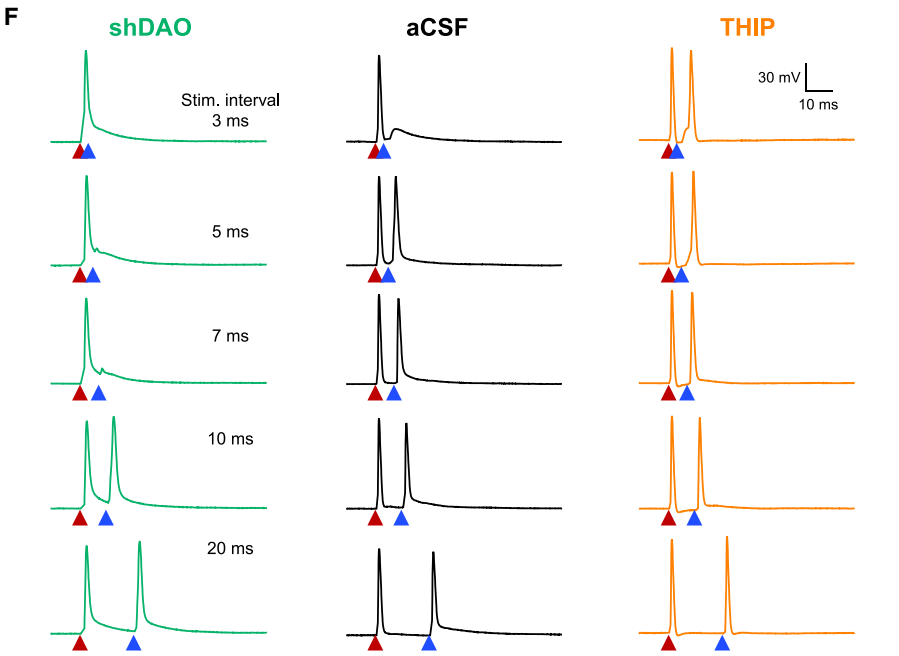

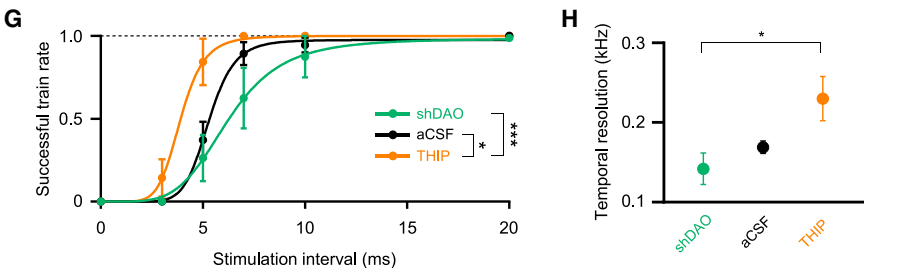

(legend on next page)

Please cite this article in press as: Kwak et al., Astrocytes Control Sensory Acuity via Tonic Inhibition in the Thalamus, Neuron (2020), https://doi.org/10.1016/j.neuron.2020.08.013

not cause changes in locomotion (Figure 7H). For evaluation of improvement in tactile discrimination by THIP, we used a smaller difference in texture (ΔG = 80) (Figure 7G). The DI of the control was nearly zero, whereas the THIP group showed a significantly higher DI (Figure 7I). These results suggest that the increase of tonic current of VB neurons improves tactile acuity without changing short-term memory (Figure 7J).

Altogether, we demonstrated that bidirectional modulation of the tonic GABA current, either with reduction of tonic GABA (shDAO, shAldh1a1, and shBest1) or with increase in tonic GABA (THIP), can impair or enhance tactile discrimination, respectively. This conclusion is evident with a positive correlation between the performance index in tactile discrimination ($G_{max}/\Delta G$) and the tonic current, temporal resolution, and spike discrimination performance (Figure 7K), mechanistically supported by negative correlations between the performance index and the spike probability, spike latency, and jitter of TC neurons (Figure 7K). Overall, our results indicate that the physiological role of tonic GABA in VB is to dynamically control tactile acuity.

DISCUSSION

Putrescine-DAO-Aldh1a1-Best1 Axis as the New Metabolic Axis

Our study identifies the duo of DAO and Aldh1a1 as the GABA-synthesizing enzymes, which degrades a diamine, putrescine, in two metabolic steps (Figure S7G). Although abundant in the brain, putrescine's function in the brain has been largely ignored. Since the first report of the catabolic pathway from putrescine to GABA (Seiler and Al-Therib, 1974), the MAO-B-dependent four-step putrescine degradation pathway has been reported to produce GABA in the cerebellar (Yoon et al., 2014), the striatal (Yoon et al., 2014), the hippocampal (Jo et al., 2014), and the substantia nigral (Heo et al., 2020) astrocytes. The level of astrocytic putrescine appears to be positively linked to the level of astrocytic GABA and tonic GABA inhibition in the cerebellum and hippocampus (Yoon et al., 2014) as well as in the thalamus (Figure 2B), suggesting that the level of astrocytic putrescine can be a critical determinant of the level of tonic GABA. The present study has expanded the previous findings and showed that the thalamic astrocytes degrade putrescine with two enzymes, DAO and Aldh1a1, in a two-step process (Figure 3K). These differences in enzymes provide novel molecular targets to differentially control the thalamic astrocytes over other astrocytes.

The unique metabolic axis, the putrescine-DAO-Aldh1a1-Best1 axis in thalamic astrocytes, suggests that astrocytes in various regions employ diverse amine oxidases to synthesize GABA, whereas neurons mainly use GAD. This enzymatic heterogeneity in different astrocytes supports the idea of astrocytic diversities (Khakh and Deneen, 2019; Verkhratsky et al., 2019). Therefore, these findings propose a new set of determining molecular markers for the regional diversity of astrocytes in the brain.

Astrocyte as the Major Dynamic, as well as Homeostatic Regulator, of Tonic GABA

Traditionally, tonic GABA in TC neurons has been believed to originate from GABAergic TRN neurons (Herd et al., 2013). However, we provided evidence that the tonic GABA is mainly from astrocytes. Lower-tonic GABA in astrocytic Ca^{2+} chelation than in Best1 KO or KD suggests additional Ca^{2+}-dependent GABA release from thalamic astrocytes other than Best1, maybe Best3 (Golubinskaya et al., 2019). The Ca^{2+}-independent mechanism, e.g., astrocytic volume-regulated anion channel (VRAC) (Han et al., 2019; Wilson and Mongin, 2019), and/or another cellular source may also account for the remaining tonic GABA. These possibilities should be investigated.

Astrocyte can also dynamically regulate tonic GABA by expressing various neuromodulator receptors, including ARs (Verkhratsky, 2008) (Figure 4), with various Ca^{2+} kinetics (Vilardaga, 2010). Furthermore, we observed diverse patterns of tonic GABA current (steady-state and oscillation) by astrocytic Orai activation, which could be attributed to the diversity of Ca^{2+} kinetics. Such diverse Ca^{2+} kinetics and subsequent GABA release from astrocytes could exert differential temporal effects onto neighboring neurons. Dynamicity and diversity in the tonic GABA current can be reinforced spatially by heterogeneous expression of astrocytic receptors and Best1 in subcellular compartments (Jo et al., 2014; Park et al., 2013). This could induce a spatially restricted Ca^{2+} transient and GABA release, leading to a distinct mode of spatial neuromodulation at restricted neuronal compartments. We have witnessed that the astrocytic tonic GABA in the thalamus showed a postsynaptic effect, but not a presynaptic effect, suggesting that the astrocytic receptors that lead to GABA release via Ca^{2+} and Best1 are apposed to postsynaptic sites.

Altogether, we have established that astrocytes are the master regulator of extracellular GABA, which is consistent with the perspective that astrocytes can actively regulate synaptic transmission (Volterra et al., 2014), in addition to the homeostatic functions (Verkhratsky and Nedergaard, 2018).

Tonic GABA Enhances Dynamic Range and Temporal Fidelity via Postsynaptic Shunting Inhibition

The immediate action of the astrocyte-originated tonic GABA is to inhibit the synaptically evoked spike probability of TC neurons (Figures 5A–5I). Tonic GABA may inhibit neuronal excitability by presynaptic mechanisms (Berglund et al., 2016) or postsynaptic mechanisms (Brickley and Mody, 2012). We found that tonic GABA inhibits TC neurons via postsynaptic shunting inhibition, but not via presynaptic mechanisms. These results imply that

Figure 6. Tonic GABA Improves Temporal Resolution of TC Neurons

(A and B) Scheme (A) and image (B) of the sensory convergence experiment driven by two theta glasses.

(C–E) Verification of the independence of inputs by linear summation of EPSC (C) and the paired-pulse ratio (D and E). See also STAR Methods.

(F) Traces of two theta-driven spike pair generation.

(G) Curve of the successful train rate.

(H) Bar graph of the temporal resolution.

Data are presented as mean ± SEM. *$p < 0.05$; two-way ANOVA (G) and Kruskal-Wallis test (H).

Please cite this article in press as: Kwak et al., Astrocytes Control Sensory Acuity via Tonic Inhibition in the Thalamus, Neuron (2020), https://doi.org/10.1016/j.neuron.2020.08.013

CellPress

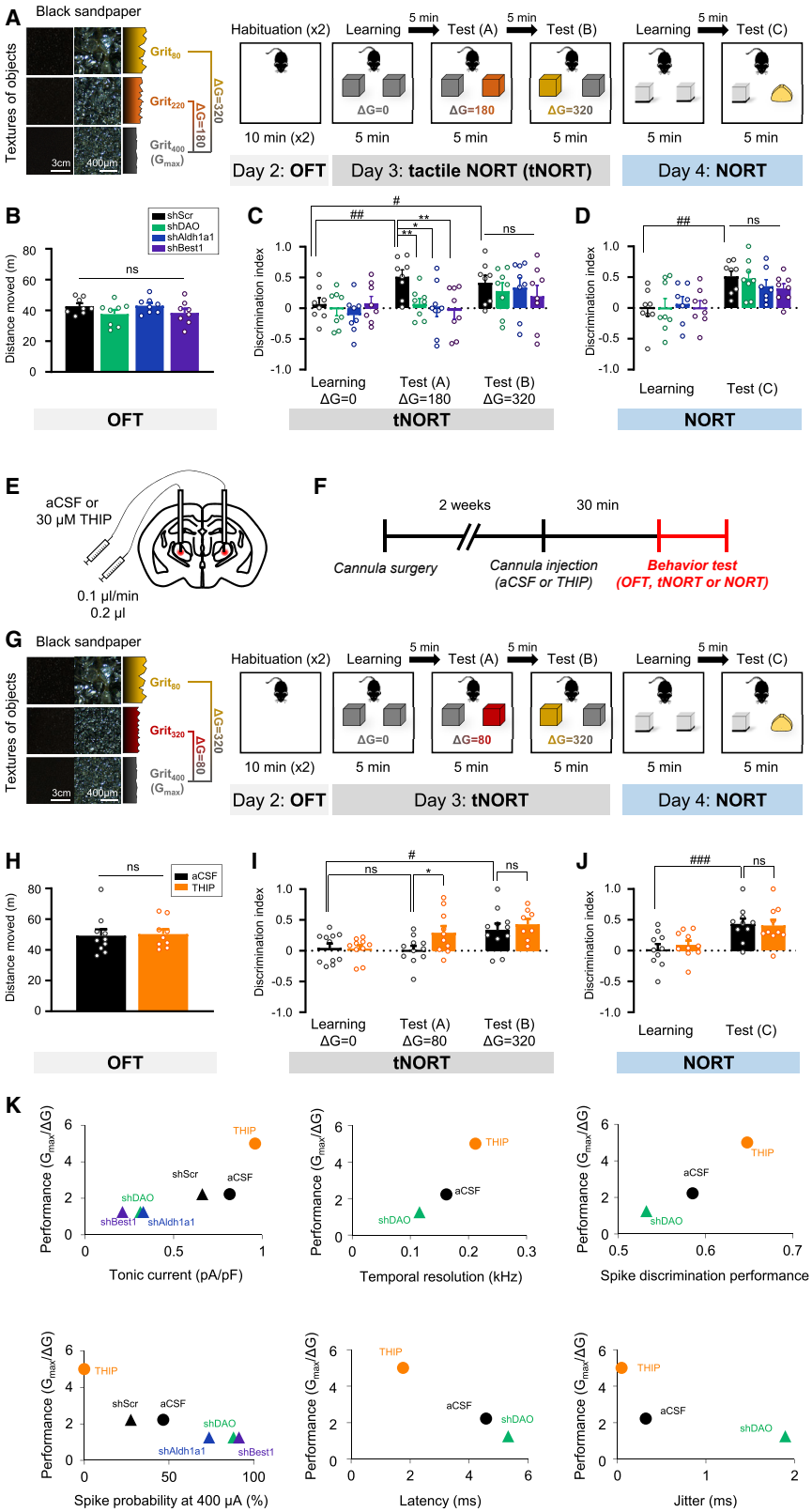

Figure 7. Tonic GABA from Astrocytes Is Critical for Tactile Discrimination

(A) Textures (left) and experimental scheme (right).

(B) Bar graph of movement in 10 min OFT.

(C and D) Summary of DI in tNORT (C) and standard NORT (D).

(E and F) Scheme (E) and timeline (F) of aCSF or THIP injection via bilateral cannulas.

(G) Textures (left) and experimental scheme (right) with cannula injection.

(H) Bar graph of movement in 10 min OFT.

(I and J) Summary of DI in tNORT (I) and standard NORT (J).

(K) Correlation between electrophysiological factors and discrimination performance.

Data are presented as mean ± SEM. Dots refer to animals.*p < 0.05; **p < 0.01; unpaired t test (B-D and H-J). #p < 0.05; ##p < 0.01; ###p < 0.001; paired t-test (B-D and H-J).

$GABA_A$Rs and $GABA_B$Rs are minimally expressed at the presynaptic terminals of the lemniscal inputs. It has been proposed that shunting inhibition serves as a gain control to reduce the amplitude of EPSPs (Eccles, 1964). However, it has been difficult to test the proposed mechanisms, because the source of shunting inhibition has been believed to be the phasic GABA and it has been technically difficult to manipulate phasic GABA release simultaneously during excitatory synaptic transmission. In this study, we have shown not only that the tonic GABA is the source of shunting inhibition in TC neurons but also that we can bidirectionally manipulate the shunting inhibition by reducing or enhancing tonic GABA.

These approaches revealed that postsynaptic shunting inhibition by tonic GABA reduces the membrane input resistance (R_m) and time constant (τ_m = RC) in the TC neuron (Figure 4U), reducing both the amplitude and the width of EPSPs. First, the decrease in EPSP amplitude renders synaptic integration less saturable, leading to an enhanced dynamic range, that is, linearity of stimulus to response of TC neurons and resulting in better discrimination of stimulation intensity by TC neurons (Figure 5). Second, the faster kinetics of EPSPs narrow the time window of synaptic integration. Therefore, only the synchronous high-frequency inputs are integrated, whereas the spurious noisy inputs are filtered out, resulting in high-temporal precision of synaptically evoked spike generation (Figure 5) and enhanced temporal resolution to discriminate independent inputs (Figure 6) and leading to enhancement of discrimination performance of TC neurons. Our study provides experimental evidence of the role of postsynaptic shunting inhibition, in which lowering of R_m and τ_m by increasing the tonic GABA paradoxically enhances the dynamic range and temporal fidelity of synaptic responses.

Tonic Inhibition Paradoxically Enhances Sensory Acuity

Tonic inhibition has been considered to exert an inhibitory role on behavior and cognition, e.g., motor coordination (Woo et al., 2018) and learning and memory in Alzheimer's disease (Jo et al., 2014). In contrast, in the thalamus, we have found that tonic inhibition paradoxically improves tactile discrimination (Figure 7). This opposite consequence can be explained by a different site of action. In the cerebellum and pathological hippocampus, high-affinity $GABA_A$Rs or $GABA_B$Rs are expressed presynaptically (Woo et al., 2018; Yarishkin et al., 2015). Activation of the presynaptic receptors exerts a strong inhibitory drive to the local circuit, resulting in an inhibitory effect in cognition. In contrast, in the thalamus, high-affinity $GABA_A$Rs mediate shunting inhibition postsynaptically, resulting in enhanced tactile discrimination. Therefore, the difference in behavioral consequences appears to come from the site of action by the tonic GABA.

In summary, we propose a model of how tonic GABA is involved in sensory acuity: When a mouse explores a novel object, the mouse pays attention to the object by activating LC to stimulate tonic GABA release from the thalamic astrocytes to enhance dynamic range and temporal fidelity of TC neurons and thus to improve discrimination between two textures. This model is supported by studies reporting that NE input from LC modulates whisker-evoked spike and the signal-to-noise ratio (SNR) (Hirata et al., 2006), as well as feature selectivity and sensory discrimination (Rodenkirch et al., 2019). Altogether, our study provides evidence that the thalamic astrocytes are the major regulators of sensory acuity via tonic inhibition.

STAR★METHODS

Detailed methods are provided in the online version of this paper and include the following:

- KEY RESOURCES TABLE
- RESOURCE AVAILABILITY
  - Lead Contact
  - Materials Availability
  - Data and Code Availability
- EXPERIMENTAL MODEL AND SUBJECT DETAILS
  - Animals
- METHOD DETAILS
  - Preparation of gene-specific shRNA and shRNA virus
  - Virus injection
  - Preparation of brain slices
  - Recording of gabazine-sensitive currents in brain slice
  - Recording of synaptically evoked EPSP and spike
  - Recording of action potential generation by current injection
  - Electrophysiology data analysis
  - Norepinephrine imaging in thalamus
  - Brain slice Ca^{2+} imaging in VB astrocytes
  - Immunohistochemistry
  - Image quantification
  - Immunogold electron microscopy
  - Enzyme inhibition assay
  - Primary astrocyte culture
  - Quantitative RT-PCR
  - Cultured astrocyte Ca^{2+} imaging
  - Sniffer-patch with primary astrocyte
  - Immunocytochemistry
  - Metabolite analysis
  - Sniffer-patch with acutely dissociated astrocyte
  - Discrimination performance algorithm using spike count histogram
  - Temporal fidelity analysis
  - Temporal discrimination and temporal resolution of two inputs converging onto a single VB TC neuron
  - Population synchrony analysis
  - Novel object recognition test (NORT)
  - Tactile NORT (tNORT)
  - Standard NORT (NORT)
  - Cannula injection
  - Calculation of THIP concentration for THIP infusion *in vivo*
- QUANTIFICATION AND STATISTICAL ANALYSIS

SUPPLEMENTAL INFORMATION

Supplemental Information can be found online at https://doi.org/10.1016/j.neuron.2020.08.013.

ACKNOWLEDGMENTS

This research was supported by the National Research Foundation of Korea (NRF) (2017R1A5A2015391, 2014M3A7B4051596, 2017R1A2B3011098, 2017M3C7A1023471, 2015R1A3A2066619, 2013M3A9C4078145, and 2020R1A4A1019009), the Korea Health Technology R&D Project of the Korea Health Industry Development Institute (HI18C1664), the International Collaborative R&D Program funded by the Ministry of Trade, Industry and Energy (N0001720), the General Research Program of the National Natural Science Foundation of China (31871087 and 31671118), Brain Korea 21 PLUS, and Institute for Basic Science (IBS), Center for Cognition and Sociality (IBS-R001-D2).

AUTHOR CONTRIBUTIONS

H.K., W.K., Sangwoo Kim, K.S., J.-I.S., J.M.L., E.H.L., J.Y.B., G.E.H., J.-E.O., Y.M.P., Sunpil Kim, J.F., S.E.L., J.W.C., K.H.K., Y.S.K., J.W, D.L., T.S., and S.W.K. performed experiments. K.D.P., B.-E.Y., J.L., Y.L., H.L., Y.C.B., C.J.L., and E.C. supervised the analysis and manuscript.

DECLARATION OF INTERESTS

The authors declare no competing interests.

Received: March 11, 2020
Revised: July 5, 2020
Accepted: August 14, 2020
Published: September 8, 2020

REFERENCES

Bar El, Y., Kanner, S., Barzilai, A., and Hanein, Y. (2018). Activity changes in neuron-astrocyte networks in culture under the effect of norepinephrine. PLoS ONE *13*, e0203761.

Belelli, D., Peden, D.R., Rosahl, T.W., Wafford, K.A., and Lambert, J.J. (2005). Extrasynaptic GABAA receptors of thalamocortical neurons: a molecular target for hypnotics. J. Neurosci. *25*, 11513–11520.

Berglund, K., Wen, L., Dunbar, R.L., Feng, G., and Augustine, G.J. (2016). Optogenetic Visualization of Presynaptic Tonic Inhibition of Cerebellar Parallel Fibers. J. Neurosci. *36*, 5709–5723.

Brickley, S.G., and Mody, I. (2012). Extrasynaptic GABA(A) receptors: their function in the CNS and implications for disease. Neuron *73*, 23–34.

Castro-Alamancos, M.A. (2002). Properties of primary sensory (lemniscal) synapses in the ventrobasal thalamus and the relay of high-frequency sensory inputs. J. Neurophysiol. *87*, 946–953.

Dana, H., Mohar, B., Sun, Y., Narayan, S., Gordus, A., Hasseman, J.P., Tsegaye, G., Holt, G.T., Hu, A., Walpita, D., et al. (2016). Sensitive red protein calcium indicators for imaging neural activity. eLife *5*, e12727.

Deschênes, M., Timofeeva, E., and Lavallée, P. (2003). The relay of high-frequency sensory signals in the Whisker-to-barreloid pathway. J. Neurosci. *23*, 6778–6787.

Ding, F., O'Donnell, J., Thrane, A.S., Zeppenfeld, D., Kang, H., Xie, L., Wang, F., and Nedergaard, M. (2013). α1-Adrenergic receptors mediate coordinated Ca2+ signaling of cortical astrocytes in awake, behaving mice. Cell Calcium *54*, 387–394.

Eccles, J.C. (1964). The Physiology of Synapses (Springer-Verlag).

Evans, R., Deng, Z., Rogerson, A.K., McLachlan, A.S., Richards, J.J., Nilsson, M., and Morris, G.A. (2013). Quantitative interpretation of diffusion-ordered NMR spectra: can we rationalize small molecule diffusion coefficients? Angew. Chem. Int. Ed. Engl. *52*, 3199–3202.

Evans, R., Dal Poggetto, G., Nilsson, M., and Morris, G.A. (2018). Improving the Interpretation of Small Molecule Diffusion Coefficients. Anal. Chem. *90*, 3987–3994.

Feng, J., Zhang, C., Lischinsky, J.E., Jing, M., Zhou, J., Wang, H., Zhang, Y., Dong, A., Wu, Z., Wu, H., et al. (2019). A Genetically Encoded Fluorescent Sensor for Rapid and Specific *In Vivo* Detection of Norepinephrine. Neuron *102*, 745–761.

Finger, S. (1972). Lemniscal and extralemniscal thalamic lesions and tactile discrimination in the rat. Exp. Brain Res. *15*, 532–542.

Fonnum, F., and Walberg, F. (1973). The concentration of GABA within inhibitory nerve terminals. Brain Res. *62*, 577–579.

Fritsch, F.N., and Carlson, R.E. (1980). Monotone Piecewise Cubic Interpolation. SIAM J. Numer. Anal. *17*, 238–246.

Golubinskaya, V., Vontell, R., Supramaniam, V., Wyatt-Ashmead, J., Gustafsson, H., Mallard, C., and Nilsson, H. (2019). Bestrophin-3 Expression in a Subpopulation of Astrocytes in the Neonatal Brain After Hypoxic-Ischemic Injury. Front. Physiol. *10*, 23.

Han, Y.E., Kwon, J., Won, J., An, H., Jang, M.W., Woo, J., Lee, J.S., Park, M.G., Yoon, B.E., Lee, S.E., et al. (2019). Tweety-homolog (*Ttyh*) Family Encodes the Pore-forming Subunits of the Swelling-dependent Volume-regulated Anion Channel ($VRAC_{swell}$) in the Brain. Exp. Neurobiol. *28*, 183–215.

Heo, J.Y., Nam, M.H., Yoon, H.H., Kim, J., Hwang, Y.J., Won, W., Woo, D.H., Lee, J.A., Park, H.J., Jo, S., et al. (2020). Aberrant Tonic Inhibition of Dopaminergic Neuronal Activity Causes Motor Symptoms in Animal Models of Parkinson's Disease. Curr. Biol. *30*, 276–291.e9.

Herd, M.B., Brown, A.R., Lambert, J.J., and Belelli, D. (2013). Extrasynaptic GABA(A) receptors couple presynaptic activity to postsynaptic inhibition in the somatosensory thalamus. J. Neurosci. *33*, 14850–14868.

Hirata, A., Aguilar, J., and Castro-Alamancos, M.A. (2006). Noradrenergic activation amplifies bottom-up and top-down signal-to-noise ratios in sensory thalamus. J. Neurosci. *26*, 4426–4436.

Hougaard, D.M., Houen, G., and Larsson, L.I. (1992). Regulation of gastric mucosal diamine oxidase activity by gastrin. FEBS Lett. *307*, 135–138.

Jiménez-González, C., Pirttimaki, T., Cope, D.W., and Parri, H.R. (2011). Non-neuronal, slow GABA signalling in the ventrobasal thalamus targets δ-subunit-containing GABA(A) receptors. Eur. J. Neurosci. *33*, 1471–1482.

Jo, S., Yarishkin, O., Hwang, Y.J., Chun, Y.E., Park, M., Woo, D.H., Bae, J.Y., Kim, T., Lee, J., Chun, H., et al. (2014). GABA from reactive astrocytes impairs memory in mouse models of Alzheimer's disease. Nat. Med. *20*, 886–896.

Jung, J.Y., Lee, S.E., Hwang, E.M., and Lee, C.J. (2016). Neuronal Expression and Cell-Type-Specific Gene-Silencing of Best1 in Thalamic Reticular Nucleus Neurons Using pSico-Red System. Exp. Neurobiol. *25*, 120–129.

Kao, C.Q., and Coulter, D.A. (1997). Physiology and pharmacology of corticothalamic stimulation-evoked responses in rat somatosensory thalamic neurons *in vitro*. J. Neurophysiol. *77*, 2661–2676.

Khakh, B.S., and Deneen, B. (2019). The Emerging Nature of Astrocyte Diversity. Annu. Rev. Neurosci. *42*, 187–207.

Kim, J.I., Ganesan, S., Luo, S.X., Wu, Y.W., Park, E., Huang, E.J., Chen, L., and Ding, J.B. (2015). Aldehyde dehydrogenase 1a1 mediates a GABA synthesis pathway in midbrain dopaminergic neurons. Science *350*, 102–106.

Koh, W., Park, Y.M., Lee, S.E., and Lee, C.J. (2017). AAV-Mediated Astrocyte-Specific Gene Expression under Human *ALDH1L1* Promoter in Mouse Thalamus. Exp. Neurobiol. *26*, 350–361.

Kyung, T., Lee, S., Kim, J.E., Cho, T., Park, H., Jeong, Y.M., Kim, D., Shin, A., Kim, S., Baek, J., et al. (2015). Optogenetic control of endogenous Ca(2+) channels *in vivo*. Nat. Biotechnol. *33*, 1092–1096.

Lee, S., Yoon, B.E., Berglund, K., Oh, S.J., Park, H., Shin, H.S., Augustine, G.J., and Lee, C.J. (2010). Channel-mediated tonic GABA release from glia. Science *330*, 790–796.

Maex, R., and De Schutter, E. (1998). Synchronization of golgi and granule cell firing in a detailed network model of the cerebellar granule cell layer. J. Neurophysiol. *80*, 2521–2537.

Marmorstein, L.Y., Wu, J., McLaughlin, P., Yocom, J., Karl, M.O., Neussert, R., Wimmers, S., Stanton, J.B., Gregg, R.G., Strauss, O., et al. (2006). The light peak of the electroretinogram is dependent on voltage-gated calcium channels and antagonized by bestrophin (best-1). J. Gen. Physiol. *127*, 577–589.

McCormick, D.A., and Bal, T. (1994). Sensory gating mechanisms of the thalamus. Curr. Opin. Neurobiol. *4*, 550–556.

McGlone, F., Wessberg, J., and Olausson, H. (2014). Discriminative and affective touch: sensing and feeling. Neuron *82*, 737–755.

Morgan, C.A., Parajuli, B., Buchman, C.D., Dria, K., and Hurley, T.D. (2015). N,N-diethylaminobenzaldehyde (DEAB) as a substrate and mechanism-based inhibitor for human ALDH isoenzymes. Chem. Biol. Interact. *234*, 18–28.

Park, H., Han, K.S., Oh, S.J., Jo, S., Woo, J., Yoon, B.E., and Lee, C.J. (2013). High glutamate permeability and distal localization of Best1 channel in CA1 hippocampal astrocyte. Mol. Brain *6*, 54.

Park, J.-H., Ju, Y.H., Choi, J.W., Song, H.J., Jang, B.K., Woo, J., Chun, H., Kim, H.J., Shin, S.J., Yarishkin, O., et al. (2019). Newly developed reversible MAO-B inhibitor circumvents the shortcomings of irreversible inhibitors in Alzheimer's disease. Sci. Adv. *5*, eaav0316.

Passaquin, A.C., Schreier, W.A., and de Vellis, J. (1994). Gene expression in astrocytes is affected by subculture. Int. J. Dev. Neurosci. *12*, 363–372.

Pinault, D. (2004). The thalamic reticular nucleus: structure, function and concept. Brain Res. Brain Res. Rev. *46*, 1–31.

Rodenkirch, C., Liu, Y., Schriver, B.J., and Wang, Q. (2019). Locus coeruleus activation enhances thalamic feature selectivity via norepinephrine regulation of intrathalamic circuit dynamics. Nat. Neurosci. *22*, 120–133.

Schwarz, L.A., and Luo, L. (2015). Organization of the locus coeruleus-norepinephrine system. Curr. Biol. *25*, R1051–R1056.

Seiler, N., and Al-Therib, M.J. (1974). Putrescine catabolism in mammalian brain. Biochem. J. *144*, 29–35.

Serrano, A., Haddjeri, N., Lacaille, J.C., and Robitaille, R. (2006). GABAergic network activation of glial cells underlies hippocampal heterosynaptic depression. J. Neurosci. *26*, 5370–5382.

Sherman, S.M. (2001). Tonic and burst firing: dual modes of thalamocortical relay. Trends Neurosci. *24*, 122–126.

Srinivasan, R., Lu, T.Y., Chai, H., Xu, J., Huang, B.S., Golshani, P., Coppola, G., and Khakh, B.S. (2016). New Transgenic Mouse Lines for Selectively Targeting Astrocytes and Studying Calcium Signals in Astrocyte Processes *In Situ* and *In Vivo*. Neuron *92*, 1181–1195.

Stell, B.M., and Mody, I. (2002). Receptors with different affinities mediate phasic and tonic GABA(A) conductances in hippocampal neurons. J. Neurosci. *22*, RC223.

Urbain, N., Salin, P.A., Libourel, P.A., Comte, J.C., Gentet, L.J., and Petersen, C.C.H. (2015). Whisking-Related Changes in Neuronal Firing and Membrane Potential Dynamics in the Somatosensory Thalamus of Awake Mice. Cell Rep. *13*, 647–656.

Verkhratsky, A. (2008). Neurotransmitter Receptors in Astrocytes. In Astrocytes in (Patho)Physiology of the Nervous System, V. Parpura and P.G. Haydon, eds. (Springer Science + Business Media), pp. 49–67.

Verkhratsky, A., and Nedergaard, M. (2018). Physiology of Astroglia. Physiol. Rev. *98*, 239–389.

Verkhratsky, A., Rodrigues, J.J., Pivoriunas, A., Zorec, R., and Semyanov, A. (2019). Astroglial atrophy in Alzheimer's disease. Pflugers Arch. *471*, 1247–1261.

Vilardaga, J.P. (2010). Theme and variations on kinetics of GPCR activation/deactivation. J. Recept. Signal Transduct. Res. *30*, 304–312.

Volterra, A., Liaudet, N., and Savtchouk, I. (2014). Astrocyte Ca^{2+} signalling: an unexpected complexity. Nat. Rev. Neurosci. *15*, 327–335.

Waiblinger, C., Whitmire, C.J., Sederberg, A., Stanley, G.B., and Schwarz, C. (2018). Primary Tactile Thalamus Spiking Reflects Cognitive Signals. J. Neurosci. *38*, 4870–4885.

Wang, Q., Webber, R.M., and Stanley, G.B. (2010). Thalamic synchrony and the adaptive gating of information flow to cortex. Nat. Neurosci. *13*, 1534–1541.

Wilson, C.S., and Mongin, A.A. (2019). The signaling role for chloride in the bidirectional communication between neurons and astrocytes. Neurosci. Lett. *689*, 33–44.

Woo, D.H., Han, K.S., Shim, J.W., Yoon, B.E., Kim, E., Bae, J.Y., Oh, S.J., Hwang, E.M., Marmorstein, A.D., Bae, Y.C., et al. (2012). TREK-1 and Best1 channels mediate fast and slow glutamate release in astrocytes upon GPCR activation. Cell *151*, 25–40.

Woo, J., Min, J.O., Kang, D.S., Kim, Y.S., Jung, G.H., Park, H.J., Kim, S., An, H., Kwon, J., Kim, J., et al. (2018). Control of motor coordination by astrocytic tonic GABA release through modulation of excitation/inhibition balance in cerebellum. Proc. Natl. Acad. Sci. USA *115*, 5004–5009.

Wu, H.P., Ioffe, J.C., Iverson, M.M., Boon, J.M., and Dyck, R.H. (2013). Novel, whisker-dependent texture discrimination task for mice. Behav. Brain Res. *237*, 238–242.

Wu, Z., Guo, Z., Gearing, M., and Chen, G. (2014). Tonic inhibition in dentate gyrus impairs long-term potentiation and memory in an Alzheimer's [corrected] disease model. Nat. Commun. *5*, 4159.

Yang, J., Cheng, Q., Takahashi, A., and Goubaeva, F. (2006). Kinetic properties of GABA rho1 homomeric receptors expressed in HEK293 cells. Biophys. J. *91*, 2155–2162.

Yarishkin, O., Lee, J., Jo, S., Hwang, E.M., and Lee, C.J. (2015). Disinhibitory Action of Astrocytic GABA at the Perforant Path to Dentate Gyrus Granule Neuron Synapse Reverses to Inhibitory in Alzheimer's Disease Model. Exp. Neurobiol. *24*, 211–218.

Yoon, B.E., Woo, J., Chun, Y.E., Chun, H., Jo, S., Bae, J.Y., An, H., Min, J.O., Oh, S.J., Han, K.S., et al. (2014). Glial GABA, synthesized by monoamine oxidase B, mediates tonic inhibition. J. Physiol. *592*, 4951–4968.

Yu, X., Taylor, A.M.W., Nagai, J., Golshani, P., Evans, C.J., Coppola, G., and Khakh, B.S. (2018). Reducing Astrocyte Calcium Signaling *In Vivo* Alters Striatal Microcircuits and Causes Repetitive Behavior. Neuron *99*, 1170–1187.

Please cite this article in press as: Kwak et al., Astrocytes Control Sensory Acuity via Tonic Inhibition in the Thalamus, Neuron (2020), https://doi.org/10.1016/j.neuron.2020.08.013

STAR★METHODS

KEY RESOURCES TABLE

REAGENT or RESOURCE	SOURCE	IDENTIFIER
Antibodies		
Rabbit anti-Best1 antibody	Produced from Abfrontier	N/A
Guinea-pig anti-GABA antibody	Millipore	AB175; RRID: AB_91011
Rabbit anti-Aldh1l1 antibody	Novus	NBP2-25143; RRID: AB_2864305
Mouse anti-NeuN antibody	Millipore	MAB377; RRID: AB_2298772
Rabbit anti-S100β antibody	Abcam	Ab41548; RRID: AB_956280
Rabbit anti-putrescine antibody	Cloud-Clone	PAX051Ge01; RRID: AB_2864306
Rabbit anti-DAO antibody	Novus Biologicals	NBP1-58006; RRID: AB_11022358
Rabbit anti-MAO-B antibody	Sigma-Aldrich	HPA002328; RRID: AB_1854062
Rabbit anti-Aldh1a1 antibody	Abcam	Ab52492; RRID: AB_867566
Rabbit anti-GAD65/67 antibody	Millipore	AB1511; RRID: AB_90715
Chicken anti-GFP antibody	Abcam	Ab13970. RRID: AB_300798
Bacterial and Virus Strains		
AAV-pSico-Red Scrambled-shRNA virus	KIST virus facility	N/A
AAV-pSico-Red Best1 shRNA virus	KIST virus facility	N/A
AAV-pSico-Red DAO shRNA virus	KIST virus facility	N/A
AAV-pSico-Red Aldh1a1 shRNA virus	KIST virus facility	N/A
AAV-hAldh1l1-Cre virus	KIST virus facility	N/A
AAV-FLEX-jRCaMP1a virus	KIST virus facility	N/A
Lenti-DIO-optoSTIM1 virus	IBS virus facility	N/A
AAV-GFAP104-GRAB$_{NE2m}$ virus	IBS virus facility	N/A
Chemicals, Peptides, and Recombinant Proteins		
TFLLR-NH2	Peptron	N/A
Tamoxifen	Sigma-Aldrich	T5648
Concanamycin A	Sigma-Aldrich	C9705
Gabazine	Sigma-Aldrich	S106
D-APV	Tocris	0106
CNQX disodium salt hydrate	Sigma-Aldrich	C239
Tetrodotoxin	ALOMONE	T-550
Lidocaine N-ethyl Bromide (QX314)	Sigma-Aldrich	L5783
Recombinant human DAO (ABP1/AOC1) protein	R&D Systems	8298-AO
Recombinant human MAO-B protein	Sigma-Aldrich	M7441
Safinamide	Produced from KIST	N/A
Aminoguanidine hydrochloride	Sigma-Aldrich	396494
4-Diethylaminobenzaldehyde	Sigma-Aldrich	D86256
Disulfiram	Sigma-Aldrich	PHR1690
Selegiline	Sigma-Aldrich	M003
Nipecotic acid (NPA)	Sigma-Aldrich	211672
NO-711 hydrochloride	Sigma-Aldrich	N142
(S)-SNAP-5114	Sigma-Aldrich	S1069
4,5,6,7-Tetrahydroisoxazolo[5,4-c]pyridin-3-ol hydrochloride (THIP hydrochloride)	Sigma-Aldrich	T101
CGP55845 hydrochloride	Sigma-Aldrich	SML0594
(±)-Norepinephrine (+)-bitartrate salt	Sigma-Aldrich	A0937

(*Continued on next page*)

Please cite this article in press as: Kwak et al., Astrocytes Control Sensory Acuity via Tonic Inhibition in the Thalamus, Neuron (2020), https://doi.org/10.1016/j.neuron.2020.08.013

Continued

REAGENT or RESOURCE	SOURCE	IDENTIFIER
Prazosin hydrochloride	Sigma-Aldrich	P7791
Phenylephrine hydrochloride	Sigma-Aldrich	P6126
U73122	Tocris	1268
1,2-Bis(2-Aminophenoxy)ethane-N,N,N',N'-tetraacetic acid (BAPTA)	Sigma-Aldrich	A4926
Alexa fluor 488 hydrazide, sodium salt	Thermofischer Scientific	A10436
Picrotoxin (PTX)	Tocris	1128
Critical Commercial Assays		
Amplex Red Monoamine oxidase Assay Kit	Molecular Probes	A12214
Experimental Models: Cell Lines		
Human: HEK293T cells	ATCC	CRL-3216; RRID:CVCL_0063
Experimental Models: Organisms/Strains		
Mouse: BALB/C Best1^{tm1Lmar}/Best1^{tm1Lmar}	From Dr. Alan D. Marmorstein (Marmorstein et al., 2006)	RRID:MGI:3797408
Mouse: FVB/N-Tg(GFAPGFP)14Mes/J	Jackson	JAX stock #003257; RRID: IMSR_JAX:003257
Mouse: Tg(Aldh1l1-EGFP)OFC789Gsat/Mmucd	MMRRC	RRID:MMRRC_011015-UCD
Mouse: B6N.FVB-Tg(Aldh1l1-cre/ERT2)1Khakh/J	From Dr. Baljit S. Khakh (Srinivasan et al., 2016)	JAX stock #031008; RRID: IMSR_JAX:031008
Mouse: B6.Cg-Gt(ROSA)26Sor$^{tm14(CAG-tdTomato)Hze}$/J	Jackson	JAX stock #007914; RRID: IMSR_JAX:007914
Oligonucleotides		
shRNA targeting sequence: Best1: TTTGCCAACTTGTCAATGAA	Woo et al., 2012	N/A
shRNA targeting sequence: DAO: AGATTCTTGGATGACTCCAGC	This paper	N/A
shRNA targeting sequence: Aldh1a1: TTTCCCACCATTGAGTGCC	Kim et al., 2015	N/A
shRNA targeting sequence: MAO-B: AATCGTAAGATACGATTCTGG	Jo et al., 2014	N/A
Primer: Mouse Gapdh qRT-F; GCC AAG GTC ATC CAT GAC AAC T	This paper	N/A
Primer: Mouse Gapdh qRT-R; GAG GGG CCA TCC ACA GTC T	This paper	N/A
Primer: Mouse Dao qRT-F; ATC TGC TGT GAC GAC TCC TC	This paper	N/A
Primer: Mouse Dao qRT-R; TGG CCA AAG TCA GAT TCT TGG	This paper	N/A
Primer: Mouse Aldh1a1 qRT-F; ATG GAT GCT TCA GAG AGG GG	This paper	N/A
Primer: Mouse Aldh1a1 qRT-R; ATG CAG CCT CCT AAA TCC GA	This paper	N/A
Primer: Mouse Mao-b qRT-F; AGT TGA GCG GCT GAT ACA CT	This paper	N/A
Primer: Mouse Mao-b qRT-R; TGG CCC ATC TCA TCC ATT GT	This paper	N/A
Primer: Mouse Gfap qRT-F; GAG GGA CAA CTT TGC ACA GG	This paper	N/A
Primer: Mouse Gfap qRT-R; TCC TCC AGC GAT TCA ACC TT	This paper	N/A

(*Continued on next page*)

Please cite this article in press as: Kwak et al., Astrocytes Control Sensory Acuity via Tonic Inhibition in the Thalamus, Neuron (2020), https://doi.org/10.1016/j.neuron.2020.08.013

Continued

REAGENT or RESOURCE	SOURCE	IDENTIFIER
Primer: Mouse Aldh1l1 qRT-F; GAG GAG GTG AAG GAG CTG TG	This paper	N/A
Primer: Mouse Aldh1l1 qRT-R; GTC CTC CCC TCT CAA CTT CC	This paper	N/A
Primer: Mouse Par1 qRT-F; ACC AAC GTC CTC CTG ATT GT	This paper	N/A
Primer: Mouse Par1 qRT-R; TCG GAG GAG GCG TAG TAG TA	This paper	N/A
Recombinant DNA		
pSicoR-mCherry plasmids	Addgene	RRID:Addgene_21907
pSico-Red plasmids	Jung et al., 2016	RRID:Addgene_84882
pAAV-pSicoR Scrambled-shRNA	This paper	N/A
pAAV-pSicoR Best1 shRNA	This paper	N/A
pAAV-pSicoR DAO shRNA	This paper	N/A
pAAV-pSicoR Aldh1a1 shRNA	This paper	N/A
pAAV-pSico-Red Scrambled-shRNA	Jung et al., 2016	N/A
pAAV-pSico-Red Best1 shRNA	Jung et al., 2016	N/A
pAAV-pSico-Red DAO shRNA	This paper	N/A
pAAV-pSico-Red Aldh1a1 shRNA	This paper	N/A
pAAV-hAldh1l1-Cre	Koh et al., 2017	N/A
pAAV.CAG.Flex.NES-jRCaMP1a.WPRE.SV40	Dana et al., 2016	RRID:Addgene_100846
pLenti-DIO-optoSTIM1	Kyung et al., 2015	N/A
pAAV-GFAP104-GRAB$_{NE2m}$	From Dr. Yulong Li (Feng et al., 2019)	N/A
Software and Algorithms		
GraphPad Prism 7	GraphPad software	https://www.graphpad.com/scientific-software/prism/; RRID: SCR_015807
Imaging WorkBench 6.2	Indec BioSystems	http://www.indecbiosystems.com/imagingworkbench/default.asp; RRID: SCR_016589
ImageJ	National Institutes of Health	https://imagej.nih.gov/ij/; RRID: SCR_003070
pClamp 10.4	Molecular Devices	https://www.moleculardevices.com/products/axon-patch-clamp-system/acquisition-and-analysis-software/pclamp-software-suite; RRID: SCR_011323
Ethovision XT	Noldus	https://www.noldus.com/ethovision-xt; RRID: SCR_000441

RESOURCE AVAILABILITY

Lead Contact

Further information and requests for reagents may be directed to, and will be fulfilled by the Lead Contact, Eunji Cheong (eunjicheong@yonsei.ac.kr).

Materials Availability

This study did not generate unique reagents.

Data and Code Availability

Raw data and analysis code are available without restriction from the Lead Contact.

Please cite this article in press as: Kwak et al., Astrocytes Control Sensory Acuity via Tonic Inhibition in the Thalamus, Neuron (2020), https://doi.org/10.1016/j.neuron.2020.08.013

EXPERIMENTAL MODEL AND SUBJECT DETAILS

Animals

For experiments including Best1 KO group, male BALB/c mice (4-6-week-old) were used (RRID:MGI:3797408). Best1 KO mice (Marmorstein et al., 2006) and wild-type littermates were obtained by mating heterozygous mice with BALB/c genetic backgrounds. Genotypes were determined by PCR using the following primers: mb0601r, 5′-TGA ATG GTG ACC TCC AAG GCT ATC C-3′ ; mb9374f, 5′-AAC AAA GGG TAA GCA GGA GTG CCC-3′ ; and neo2351f, 5′-GGA AGA CAA TAG CAG GCA TGC TGG G-3′. For immunostaining, male and female Aldh1l1-EGFP transgenic mice whose genetic backgrounds is FVB were used (RRID:MMRRC_011015-UCD). Genotypes were determined by PCR using the following primers: 5′-CCT CTG GCT GCT CCT TCA ACA G-3′ ; and 5′-GGT CGG GGT AGC GGC TGA A-3′. For cell-type specific gene silencing experiments including patch-clamp, wild-type male C57BL/6J mice were used. For immunogold electron microscopy, male and female GFAP-GFP mice with FVB genetic backgrounds were used (JAX stock #003257). Genotypes were determined by PCR using the following primers: 42, 5′-CTA GGC CAC AGA ATT GAA AGA TCT-3′ ; 43, 5′-GTA GGT GGA AAT TCT AGC ATC ATC C-3′ ; 872, 5′-AAG TTC ATC TGC ACC ACC G-3′ and 1416, 5′-TCC TTG AAG AAG ATG GTG CG-3′. For acute sniffer-patch experiment, Aldh1l1-cre/ERT2 (Srinivasan et al., 2016) (JAX stock #031008) was crossed with Ai14 (JAX stock #007914) to visualize thalamic astrocyte with tdTomato reporter. For Aldh1l1-cre/ERT2 mice, genotypes were determined by PCR using the following primers: 21238, 5′-CTG TCC CTG TAT GCC TCT GG-3′ ; 21239, 5′-AGA TGG AGA AAG GAC TAG GCT ACA-3′ ; 30308, 5′-GGC AAA CGG ACA GAA GCA-3′ and 31091, 5′-CTT CAA CAG GTG CCT TCC A-3′. For Ai14 mice, genotypes were determined by PCR using the following primers: oIMR9020, 5′-AAG GGA GCT GCA GTG GAG TA-3′; oIMR9021, 5′-CCG AAA ATC TGT GGG AAG TC-3′; oIMR9103, 5′-GGC ATT AAA GCA GCG TAT CC-3′ and oIMR9105, 5′-CTG TTC CTG TAC GGC ATG G-3′. Both gender of the crossed mice were used in acute sniffer-patch experiment. For behavioral test, male C57BL/6J mice were used. All mice were maintained under a 12:12-h light–dark cycle (lights on 7:00 A.M.) and had *ad libitum* access to food and water. Care and handling of animals were in accordance with the guidelines of the Institutional Animal Care and Use Committee at Yonsei University (Seoul, Korea) and Korea Institute of Science and Technology (Seoul, Korea).

METHOD DETAILS

Preparation of gene-specific shRNA and shRNA virus

The shRNA sequences for scrambled, MAO-B, Aldh1a1, and Best1 were adopted from previous studies (Kim et al., 2015; Stell and Mody, 2002; Woo et al., 2012). The shRNA sequence for DAO was designed with BLOCK-iT RNAi Designer (Invitrogen, USA) and cloned into pSico and pSicoR lentiviral vectors as previously described (Woo et al., 2012). pSicoR vectors were utilized for plasmid-based shRNA expression *in vitro*. For adeno-associated-virus (AAV)-based shRNA expression *in vivo*, shRNA expression cassette was sub-cloned into pAAV-Sico-Red (pSico-Red) vector as previously reported (Jung et al., 2016). Every construct was verified with sequencing after cloning. Cloned shRNA constructs were packaged into AAV viruses in KIST Virus Facility (http://virus.kist.re.kr).

Sequence of scrambled shRNA for control: 5′-TCGCATAGCGTATGCCGTT-3′
Antisense sequence of shRNA target for MAO-B: 5′-AATCGTAAGATACGATTCTGG-3′
Antisense sequence of shRNA target for Aldh1a1: 5′-TTTCCCACCATTGAGTGCC-3′
Antisense sequence of shRNA target for Best1: 5′-TTTGCCAACTTGTCAATGAA-3′
Antisense sequence of shRNA target for DAO: 5′-AGATTCTTGGATGACTCCAGC-3′

Virus injection

Mice were anaesthetized via intraperitoneal (i.p.) injections of 2,2,2-tribromoethanol (300 mg/kg body weight; Sigma-Aldrich, USA). Viruses were bilaterally microinjected using SP100IZ syringe pump (WPI) into the VB region of the thalamus (for 3-4 week-old mice, −1.3mm lambda from bregma, ± 1.4mm lateral to the midline, −3.4 and −2.9mm ventral from the brain surface; for adult mice, −1.8mm lambda from bregma, ± 1.5mm lateral to the midline, −3.5 and −2.5mm ventral from the brain surface). Mice were used for patch-clamp 10-14 days and *in vivo* experiments 2 weeks after the virus injection.

Preparation of brain slices

Mice were anaesthetized with halothane and decapitated to remove the brain. The brains were sectioned in ice-cold slicing solution (sucrose, 234 mM; KCl, 2.5 mM; $MgSO_4$, 10 mM; NaH_2PO_4, 1.25 mM; $NaHCO_3$, 24 mM; $CaCl_2$-$2H_2O$, 0.5 mM; and glucose, 11 mM). Horizontal slices (300 μm thick) with a vibrating-knife microtome VT1000s (Leica Microsystems, Germany). For stabilization, slices were incubated in room temperature for at least 1 h in a solution containing NaCl, 124 mM; KCl, 3 mM; $MgSO_4$, 6.5 mM; NaH_2PO_4, 1.25 mM; $NaHCO_3$, 26 mM; $CaCl_2$-$2H_2O$, 1 mM; and glucose, 10 mM, and simultaneously equilibrated with 95% O_2/5% CO_2 at 25°C. In some experiments, slices were incubated with blockers while stabilization for at least 2 h. This protocol was utilized in every brain slice experiment except NE imaging.

Please cite this article in press as: Kwak et al., Astrocytes Control Sensory Acuity via Tonic Inhibition in the Thalamus, Neuron (2020), https://doi.org/10.1016/j.neuron.2020.08.013

Recording of gabazine-sensitive currents in brain slice

The gabazine (GBZ)-sensitive GABA currents were recorded under aCSF solution (NaCl, 124 mM; KCl, 3 mM; $MgSO_4$, 1.3 mM; NaH_2PO_4, 1.25 mM; $NaHCO_3$, 26 mM; $CaCl_2$-$2H_2O$, 2.4 mM; and glucose, 10 mM) aerated with 95% O_2/5% CO_2 by whole-cell voltage-clamp. Patch electrodes (4-7MΩ) fabricated from standard-wall borosilicate glass (GC150F-10, Warner Instrument Corp., USA) were filled with an intrapipette solution containing CsCl, 135 mM; HEPES, 10 mM; EGTA, 10 mM; QX-314, 5 mM; Mg-ATP, 5 mM; and Na_2-GTP, 0.5 mM, with pH adjusted to 7.3 and osmolality adjusted to 285 mOsmol/kg. Before measuring tonic current, baseline current was stabilized with D-AP5 (50 μM) and CNQX (50 μM). The amplitude of tonic GABA current was measured by the baseline shift after 10 μM GBZ application. Individual cells were visually identified using an upright Olympus EX51WI (Olympus, Japan) microscope equipped with an ORCA-R2 camera (HAMAMATSU, Japan). Signals were amplified using MultiClamp 700B (Molecular Devices, USA), and data acquisition was performed using a Digitizer 1440A and Clampex (Molecular Devices). Frequency and amplitude of spontaneous IPSCs were analyzed by Minianalysis software (Synaptosoft). For recording of optoSTIM1-evoked current, 20 Hz of 450nm-laser pulses were illuminated with a pulse width of 20 ms using MDL-III-450 (CNI laser, China). For Ca^{2+} chelating by BAPTA dialysis into thalamic astrocytes, patch pipette was filled with intrapipette solution containing CsCl, 123 mM; $MgSO_4$, 1 mM; HEPES, 10 mM; BAPTA, 10 mM; Alexa fluor 488 hydrazide, 100 μM; Mg-ATP, 5mM; and Na_2-GTP, 0.5mM, with pH adjusted to 7.35 (by CsOH) and osmolality adjusted to 282 mOsmol/kg.

Recording of synaptically evoked EPSP and spike

The synaptically evoked EPSP and spike were recorded under aCSF solution (NaCl, 130 mM; KCl, 3.5 mM; $MgCl_2$, 1.5 mM; NaH_2PO_4, 1.25 mM; $NaHCO_3$, 24 mM; $CaCl_2$, 1.5 mM; and glucose, 10 mM) aerated with 95% O_2/5% CO_2 by whole-cell current-clamp. Patch electrodes (4-7MΩ) fabricated from standard-wall borosilicate glass (GC150F-10, Warner Instrument Corp., USA) were filled with an intrapipette solution containing K-gluconate, 145 mM; HEPES, 10 mM; NaCl, 5 mM; EGTA, 0.2 mM; Mg-ATP, 5 mM; and Na_2-GTP, 0.5 mM, with pH adjusted to 7.3 and osmolality adjusted to 295 mOsmol/kg. Synaptic activity was evoked by 10 stimuli of lemniscal afferent fiber (0.1 ms, 50 μA~1000 μA, 0.1 Hz or 100 Hz) using a tungsten bipolar electrode. Spike probability was calculated as the ratio of the number of spike generation to the total number of stimuli.

Recording of action potential generation by current injection

For measurement of intrinsic firing property with or without GABA blockers or NE, the composition of extracellular buffer aCSF was following: NaCl, 130 mM; KCl, 3.5 mM; $MgCl_2$, 1.5 mM; NaH_2PO_4, 1.25 mM; $NaHCO_3$, 24 mM; $CaCl_2$, 1.5 mM; and glucose, 10 mM, aerated with 95% O_2/5% CO_2. Patch electrodes (4-7MΩ) fabricated from standard-wall borosilicate glass (GC150F-10, Warner Instrument Corp., USA) were filled with an intrapipette solution containing K-gluconate, 145 mM; HEPES, 10 mM; NaCl, 5 mM; EGTA, 0.2 mM; Mg-ATP, 5 mM; and Na_2-GTP, 0.5 mM, with pH adjusted to 7.3 and osmolality adjusted to 295 mOsmol/kg. Measuremet was performed in a whole-cell current-clamp configuration, with no membrane potential adjustment. Spikes generated by T-type Ca^{2+} channel activity were excluded in analysis and each firing rate generated by 1 s current injection was normalized to the firing rate of control firing rate. The amplitude of the current injection was determined to generate 5 to 20 spikes in control group.

Electrophysiology data analysis

The normality test was run before data analysis. Statistical analysis was performed based on normality test and independent variable. For electrophysiological recording, cells with series resistance < 30MΩ were accepted for statistical analysis. Electrophysiological data analysis was performed using the Clampfit (Molecular Devices) and Minianalysis software (Synaptosoft Inc.). Data are presented as mean ± SEM.

Norepinephrine imaging in thalamus

2 weeks after AAV-GFAP104-$GRAB_{NE2m}$ virus injection into VB, animals were deeply anesthetized with isoflurane, followed by decapitation. The brain was quickly excised from the skull and submerged in ice-cold NMDG recovery solution (92mM NMDG, 92mM HCl, 2.5mM KCl, 1.2mM NaH_2PO_4, 30mM $NaHCO_3$, 20mM HEPES, 25mM Glucose, 5mM sodium ascorbate, pH 7.4) saturated with 95% O_2 and 5% CO_2. Transverse slices of 300 μm thickness were obtained with D.S.K LinearSlicer (Dosaka EM Co. Ltd, Japan). Slices were then transferred to an incubation chamber with artificial cerebrospinal fluid (aCSF: 130 mM NaCl, 24 mM $NaHCO_3$, 3.5 mM KCl, 1.25 mM NaH_2PO_4, 1.5 mM $CaCl_2$, 1.5 mM $MgCl_2$ and 10 mM glucose, pH 7.4) at room temperature for at least 1 hr before experiment. Brain section was placed into recording chamber upon continuous bath application of aCSF. To induce norepinephrine release, electrical stimulation (0.2ms pulse width, 1 s duration, 300 μA intensity) was delivered at various frequencies (10, 20, 50 and 100 Hz). To confirm sensor-expressing region, 1 μM NE was introduced by bath application.

Brain slice Ca^{2+} imaging in VB astrocytes

AAV-FLEX-jRCaMP1a (Dana et al., 2016) virus and AAV-hALDH1l1-cre virus were delivered to VB of 3 week-old anesthetized mice as the following coordinate. 1.3mm lambda from bregma ± 1.4mm lateral to the midline, −3.4 and −2.9mm ventral from the brain surface. More than 10 days after injection, mice were sacrificed and brain slices were prepared as described above. Imaging was acquired at 0.5 to 1 frame per second with a 60X water-immersion objective lens and a 585-nm fluorescent imaging filter. Image workbench (Indec biosystems) was utilized for image acquisition and Fiji (imageJ) was utilized for image analysis.

Please cite this article in press as: Kwak et al., Astrocytes Control Sensory Acuity via Tonic Inhibition in the Thalamus, Neuron (2020), https://doi.org/10.1016/j.neuron.2020.08.013

Immunohistochemistry

Mice were anaesthetized via intraperitoneal injection of 2,2,2-tribromoethanol (300 mg/kg, Sigma-Aldrich) and transcardially perfused with 1X PBS followed by a 4% paraformaldehyde (PFA) solution. Brains were isolated from mice and post-fixed in a 4% PFA solution overnight, followed by immersion in a 30% sucrose solution for 48 h to achieve cryoprotection. Brains mounted in OCT compound (Sakura, USA) were sliced coronally with a cryostat to obtain brain sections (40 μm) containing the ventrobasal (VB) nucleus of the thalamic region. The sections were incubated in 0.1% Tween-20 in 1X PBS for 30 min and then in blocking solution (5% normal goat serum in 1X PBS) for 1 h, followed by primary antibodies with blocking solution overnight at 4°C. After incubation with primary antibodies, sections were incubated in secondary antibodies with blocking solution for 2 h at 25°C before being mounted on microscope slides with Fluorescence Mounting Medium (DAKO, USA). The following antibodies were used: rabbit anti-Best1 (produced; 1:100; Abfrontier), rabbit anti-DAO (ARP41908, 1:500; avivasysbio), rabbit anti-Aldh1a1 (ab52492, 1:500; Abcam), rabbit anti-MAO-B (HPA002328, 1:500; Sigma), rabbit anti-putrescine (PAX051Ge01, 1:500; Cloud-Clone), rabbit anti-GAD65/67 (AB1511, 1:500; Millipore), rabbit anti-s100b (ab41548, 1:500; Abcam), mouse anti-NeuN (MAB377, 1;400; Millipore) and chicken anti-GFP (ab13970, 1:1,000; Abcam), Fluorescence images were obtained with an LSM 700 confocal microscope (Carl Zeiss, Germany).

Image quantification

Confocal microscopic images were obtained in order to quantify small molecule or enzyme expression and were analyzed using the ImageJ (NIH) program. Fluorescence intensities were calculated using the mean intensity value of each fluorescence pixels in the marker-positive area. The marker-positive area was defined by thresholding and is converted into a binary mask. The mean intensity of immunostained pixels in the binary mask was calculated.

Immunogold electron microscopy

GFAP-GFP transgenic mice weighing 20–25 g were used for this study. For tissue fixation, mice were deeply anaesthetized with sodium pentobarbital (80 mg/kg, I.P.) and perfused transcardially with 10 mL of heparinized normal saline, followed by 50 mL of a freshly prepared mixture of 4% paraformaldehyde and 0.01% or 0.5% glutaraldehyde in 0.1 M phosphate buffer (PB), at pH 7.4. The cerebellum was removed and postfixed in the same fixative for 2 h at 4°C. Sections of 60 μm were cut sagittally on a Vibratome and cryoprotected overnight in 30% sucrose in PB at 4°C. Sections were frozen on dry ice for 20 min and thawed in phosphate-buffered saline (PBS; 0.01 M, pH 7.2) to enhance penetration. They were pretreated with 1% sodium borohydride for 30 min to quench glutaraldehyde, then blocked with 3% H_2O_2 for 10 min to suppress endogenous peroxidases and then perfused/treated with 10% normal donkey serum (NDS, Jackson ImmunoResearch, West Grove, PA, USA) for 30 min to mask secondary antibody binding sites. For quantitative analysis, electron micrographs were taken at x30,000 magnification in the area (μm^2) of Bergmann glial cells showing GFP immunoreactivity from thin sections incubated with GABA antiserum for each of the three GFAP-GFP mice. To assess immunoreactivity for GABA, gold particle density (number of gold particles per unit area) of each axon terminal adjacent to astrocytes was compared with that of astrocytes. Axon terminals were considered immunopositive if gold particle density over the vesicle-containing areas was at least five times higher than that in the control axon terminals, which were defined as axon terminals containing spherical vesicles and showing an asymmetric type of synaptic contact with a prominent postsynaptic density. Immunogold labeling over mitochondrial profiles was excluded from the analysis. Measurements were performed on micrographs using a digitizing tablet and ImageJ software (NIH, Bethesda, MD, USA). Statistical analysis was performed by analysis of variance (ANOVA) and mean values were compared via Scheffe's F test. Significance was set at $p < 0.05$.

Enzyme inhibition assay

Recombinant human DAO (ABP1/AOC1) protein (R&D Systems, USA) and recombinant human MAO-B protein (Sigma, USA) were purchased and enzyme assay was performed as previously described (Jo et al., 2014). Briefly, the enzymatic activity of DAO or MAO-B was measured using an Amplex Red Monoamine oxidase Assay Kit (Molecular Probes) according to the manufacturer's instructions. First, 100 ng of rhDAO or 500 ng of rhMAO-B protein was prepared with each reaction buffer (50 mM HEPES buffer-NaOH, pH7.5 for rhDAO, 0.05 M sodium phosphate buffer-NaOH, pH7.4 for rhMAO-B) in each well of 96-well plates, with or without inhibitors. After 1 hour incubation at 37°C, the mixture of hydrogen peroxidase, Amplex red reagent, and substrate (putrescine for rhDAO, benzylamine for rhMAO-B) was added in each well. The color change was quantified by measuring fluorescence at 540nm (excitation) / 580nm (emission) with Infinite M200 PRO microplate reader (TECAN). All the conditions were performed as triplet, and an averaged value of each condition was subtracted with an average value of blank condition which is performed without enzyme and inhibitor, and every condition was normalized by the condition without inhibitor.

Primary astrocyte culture

Primary cultured astrocytes were prepared from P1-P3 of C57BL/6J mouse as previous (Stell and Mody, 2002; Woo et al., 2012). Hippocampi, cerebella and thalami were dissected, and dissociated into single cell suspension by trituration in astrocyte culture media. Astrocyte culture media consists of Dulbecco's modified Eagle's medium (DMEM, Invitrogen) supplemented with 10% heat-inactivated horse serum, 10% heat-inactivated fetal bovine serum, 2 mM glutamine, 100 units/ml penicillin–streptomycin and 25 mM glucose. Cultures were incubated in humidified 5% CO_2 incubator with 37°C. On three days *in vitro* (DIV), cultured cells were vehe-

Please cite this article in press as: Kwak et al., Astrocytes Control Sensory Acuity via Tonic Inhibition in the Thalamus, Neuron (2020), https://doi.org/10.1016/j.neuron.2020.08.013

mently washed with repeated pipetting and the media was changed to eliminate other floating cell types and debris. Primary astrocyte culture was maintained DIV 10 until the confluence. To minimize the effect of reactiveness of primary cultured astrocytes (Passaquin et al., 1994), subculture was minimally performed.

Quantitative RT-PCR

Total RNA was extracted from hippocampal and thalamic cultured astrocytes (DIV 10), using RNeasy Mini Kit (QIAGEN, USA) according to the manufacturer's instructions. First-strand cDNA was prepared with total RNA using SuperScript III First-Strand Synthesis System (Invitrogen, USA) according to the manufacturer's instructions. PCR samples were prepared with Power SYBR Green Master Mix (4367659, Applied Biosystems, USA), obtained cDNA library and gene-specific primers, which are listed as below. Real-time PCRs were performed with StepOne software v2.1 in ABI StepOnePlus systems (Applied Biosystems, USA). Thermal cycler conditions were as follows: 2 min at 50°C, 15 min at 95°C, followed by 40 cycles of 15 s at 95°C and 1 min at 60°C. The amount of targeted gene expressed was normalized to an endogenous reference gene (*Gapdh*) and relative to hippocampal samples. The formula $2^{-\Delta\Delta Ct}$ was used to calculate relative expression of target genes in thalamic astrocytes, compared to hippocampal astrocytes. PCR primers of each target gene were designed using Primer3 (http://bioinfo.ut.ee/primer3/). The followings are the sequences of utilized primers. *Gapdh* forward: 5′-GCC AAG GTC ATC CAT GAC AAC T-3′; *Gapdh* reverse: 5′-GAG GGG CCA TCC ACA GTC T-3′; *Dao* forward: 5′-ATC TGC TGT GAC GAC TCC TC-3′; *Dao* reverse: 5′-TGG CCA AAG TCA GAT TCT TGG-3′; *Aldh1a1* forward: 5′-ATG GAT GCT TCA GAG AGG GG-3′; *Aldh1a1* reverse: 5′-ATG CAG CCT CCT AAA TCC GA-3′; *Mao-b* forward: 5′-AGT TGA GCG GCT GAT ACA CT-3′; *Mao-b* reverse: 5′-TGG CCC ATC TCA TCC ATT GT-3′; *Gfap* forward: 5′-GAG GGA CAA CTT TGC ACA GG-3′; *Gfap* reverse: 5′-TCC TCC AGC GAT TCA ACC TT-3′; *Aldh1l1* forward: 5′-GAG GAG GTG AAG GAG CTG TG-3′; *Aldh1l1* reverse: 5′-GTC CTC CCC TCT CAA CTT CC-3′; *Par1* forward: 5′-ACC AAC GTC CTC CTG ATT GT-3′; *Par1* reverse: 5′-TCG GAG GAG GCG TAG TAG TA-3′.

Cultured astrocyte Ca^{2+} imaging

The day before the experiment, hippocampal and thalamic astrocytes were re-plated from culture dishes onto 12-mm glass coverslips coated with poly-D-lysine (Sigma, USA) in 24-well plates, with the density of 3-5x10^4 cells/ 500 μl/well. To monitor Ca^{2+} responses, astrocytes on coverslips were incubated with 5 μM Fura-2 AM (mixed with 5 μL of 20% Pluronic acid) (Invitrogen, USA) for 40 minutes and washed with external solution. External solution contained (in mM): 150 NaCl, 10 HEPES, 3 KCl, 2 $CaCl_2$, 2 $MgCl_2$, 5.5 glucose, pH adjusted to pH 7.3 and osmolality to 325 mOsm kg^{-1}. To obtain the ratio of 340/380, intensity in images of 510nm wavelength by 340 nm and 380 nm excitation wavelengths was detected with iXon EMCCD, DV887 (ANDOR, England), and automatically calculated with Axon Imaging Workbench version 6.1 (Axon Instruments, USA). 30uM TFLLR, an agonist for PAR1, was treated with bath application, and peak amplitude of Δ340/380 from baseline was measured.

Sniffer-patch with primary astrocyte

Sensor cells were prepared from HEK293T cells with expression of GABAc by overexpression of GABAc and green fluorescence protein (pEGFP-N1) using Effectene (QIAGEN, USA), as previously described (Jo et al., 2014; Stell and Mody, 2002). For gene-silencing, thalamic astrocytes (DIV 10) were microporated with shRNA plasmids. The day before the sniffer-patch, thalamic astrocytes were re-plated from culture dishes onto 12-mm glass coverslips coated with poly-D-lysine in 24-well plates, with the density of 2-2.5x10^4 cells/ 500 μl/well. On the day of the sniffer-patch, prepared sensor cells were re-plated on the coverslips with astrocytes, with the density of 2.5-3x10^4 cells/ 500 μl/well. Fura-2 AM loading and Ca^{2+} imaging were performed as described above. External solution contained (in mM): 150 NaCl, 10 HEPES, 3 KCl, 2 $CaCl_2$, 2 $MgCl_2$, 5.5 glucose, pH adjusted to pH 7.3 and osmolality to 325 mOsm kg^{-1}. GABAc-mediated currents from sensor cells were recorded under voltage-clamp configuration (Vh = −70mV) using an Axopatch 200A amplifier (Axon Instruments, USA), acquired with pClamp 10.2 (Molecular Devices, USA). Recording electrodes (4–7 MΩ) were filled with (mM): 140 CsCl, 0.5 $CaCl_2$, 10 HEPES, 4 Mg-ATP, 0.3 Na3-GTP, and 10 EGTA (pH adjusted to 7.3 with CsOH). Osmolality is 285–295 mOsm kg−1). To induce Ca^{2+} responses from thalamic astrocytes, 500 μM TFLLR was applied with pressure (20 lbf in^{-2}, 100ms) using Picospritzer (Parker Instrument, USA). For simultaneous recordings, Axon Imaging Workbench was synchronized with pClamp. To normalize the different expression of GABAc in sensor cells, 100 μM of GABA bath application was performed to obtain maximal GABAc current from each sensor cells. Sniffed current, which is mediated by released GABA from astrocytes, was divided by maximal GABAc current. Criteria for GABA releasing cells was defined as 2% of full activation.

Immunocytochemistry

For the pharmacologic studies, thalamic astrocytes (DIV 10) on coverslips were incubated with 100 nM selegiline, 10 nM aminoguanidine or 100 μM GABA overnight. For gene-silencing studies, thalamic astrocytes (DIV 10) were microporated with shRNA plasmids. Primary thalamic cultured astrocytes on coverslips were fixed in the mixture of 4% paraformaldehyde (sc-281692, Sigma, USA) and 0.5% glutaraldehyde (G7776, Sigma, USA) in 0.1 M phosphate buffered saline (PBS) at RT for 15 min. After fixation, the cells were washed three times for 10 min each with 0.1 M PBS. The cells were blocked with PBS containing 0.3% Triton X-100 (Sigma, USA) and 10% donkey serum (S30, Millipore, USA) for 1.5 h at room temperature. The cells were incubated overnight in a mixture of the following primary antibodies with blocking solution at 4°C on a shaker: guinea-pig anti-GABA antibody (1:1000, AB175, Millipore, USA), rabbit anti-Aldh1l1 antibody (1:500, NBP2-25143, Novus, USA). After washing three times with 0.1 M PBS, the cells were incubated with the corresponding secondary antibodies: conjugated Alexa 488 donkey anti-rabbit IgG (1:500, 711-545-152, Jackson,

Please cite this article in press as: Kwak et al., Astrocytes Control Sensory Acuity via Tonic Inhibition in the Thalamus, Neuron (2020), https://doi.org/10.1016/j.neuron.2020.08.013

USA), conjugated Alexa 647 donkey anti-guinea-pig IgG (1:500, 706-605-148, Jackson, USA), for 2 h at RT. The cells were rinsed three times in 0.1 M PBS, including DAPI solution (1:2000, Pierce) for nuclear staining in second washing step. Then the coverslips were mounted onto the slide glass (22-037-246, Thermo Scientific, USA) with fluorescence mounting solution (S3023, DAKO, USA). Images were acquired using a Nikon A1R confocal microscope and analyzed using the ImageJ program (NIH). After binary conversion, region of interest (ROI) of aldh1l1-positive astrocytes was determined. The mean intensity values of GABA and Aldh1l1 in ROI were measured. For the shRNA transfected cells, same analysis was performed with only mCherry-positive astrocytes.

Metabolite analysis

Metabolite analysis for putrescine, acetyl-GABA, and GABA was performed using electrospray ionization LC-MS/MS. The system used for the analyses was an Exion LC AD UPLC coupled with an MS/MS (Triple Quad 4500 System, AB Sciex LLC, Framingham, USA) using an Acquity® UPLC BEH HILIC column (1.7 etyl-GABA, and GA 2.1 mm x 100 mm, Waters, USA) at 30°C, controlled by Analyst 1.6.2 software (AB Sciex LP, Ontario, Canada). On the astrocyte sample pellets, 70% methanol (100 μL) was added and vortexed for 30 s. Cells were lysed by three consecutive freeze/thaw cycles using liquid nitrogen, and the lysate was centrifuged for 10 min at 20,817 x g (14,000 rpm). 5 μL of the supernatant from each sample was used for DNA normalization. DNA concentrations were analyzed using a Nano-MD UV-Vis spectrophotometer (Scinco, Seoul, Korea). 20 μL of the supernatant from each sample was added with 5 μL of internal standard (d2-GABA at a final concentration of 4 μM) and vortexed for 30 s. The mixture was evaporated to dryness at 37°C under a gentle stream of nitrogen. The residue was reconstituted with 25 μL of the mobile phase A (0.1% formic acid in acetonitrile):B (50mM ammonium formate, pH 4) = 8:2 solvent by vortexing for 30 s, and sonicating for 15 min. The initial chromatographic conditions were 80% solvent A at a flow rate of 0.4 mL·min-1. After 7 min at 20% B, solvent B was set to 95% over the next 0.5 min, and these conditions were retained for an additional 1 min. The system was then returned to the initial conditions over the next 0.5 min. The system was re-equilibrated for the next 1.5 min in the initial conditions. The total running time was 10.5 min. All samples were maintained at 7°C during the analysis, and the injection volume was 5 μL. The MS analysis was performed using ESI in positive mode. The ion spray voltage and vaporizer temperature were 5.5 kV and 380°C, respectively. The curtain gas was kept at 35 psi, and the collision gas was maintained at 8 psi. The nebulizer gas was 60 psi, while the turbo gas flow rate was 70 psi. The metabolites were detected selectively using their unique multiple reaction monitoring (MRM) pairs. The following MRM mode (Q1 → Q3) was selected: putrescine (m/z 89.062 → m/z 72.1), acetyl-GABA (m/z 146.011 → m/z 86.015) and GABA (m/z 103.979 → m/z 87.1) to monitor specific parent-to-product transitions. The standard calibration curve for each metabolite was used for absolute quantification.

Sniffer-patch with acutely dissociated astrocyte

Thalamic VB astrocyte was acutely dissociated by the mechanical protocol from horizontal brain slices of Aldh1l1-CreERT2 x Ai14 (RCL-tdTomato) mice, as previously reported as "vibrating ball" technique. In brief, 300 μm of horizontal brain slices were prepared in dissection aCSF and transferred into the chamber with normal aCSF for recovery. Dissection aCSF contained (mM): 130 NaCl, 24 $NaHCO_3$, 3.5 KCl, 1.25 NaH_2PO_4, 1 $CaCl_2$, 3 $MgCl_2$ and 10 glucose saturated with 95% O_2/ 5% CO_2, pH 7.4. Normal aCSF contained (mM): 130 NaCl, 24 $NaHCO_3$, 3.5 KCl, 1.25 NaH_2PO_4, 1.5 $CaCl_2$, 1.5 $MgCl_2$ and 10 glucose saturated with 95% O_2/ 5% CO_2, pH 7.4. Following one hour recovery in normal aCSF (with or without AG) after slicing, the slices were moved to the culture dish with astrocyte media (with or without AG) for dissociation. The vibrating (at 150 Hz) polished glass ball was moved to the surface of thalamic VB area. After the application of the vibrating ball, the astrocyte media with dissociated cells was transferred to the coverslips, with an addition of sensor cells expressing GABAc. Cells were settled at least two hours for the sniffer-patch experiments. Sniffer-patch was performed as described above.

Discrimination performance algorithm using spike count histogram

Analysis of discrimination performance was done similar to the previous study . First, the frequency histogram of spike count of each stimulus (S1, S2, S3, S4, S5 and S6) of each neuron was plotted. Then each spike count distribution was fitted to form a likelihood function (p(r|Si)) using piecewise cubic hermite Interpolating polynomial (Fritsch and Carlson, 1980). Then the probability of choosing Si when the presented stimulus was actually Sj (= p(Si|Sj) was calculated to be the area of the region of p(r|Sj) in which the p(r|Si) is maximal. The discrimination performance was defined as mean probability of correctly inferred events (when i = j, the diagonal factors in matrices).

Temporal fidelity analysis

Analysis of temporal fidelity was done only when the 9^{th} stimulus successfully generated spike within the unitary stimulation interval (10 ms in 100 hz stimulation experiment). Latency was calculated as a time lag between stimulus to peak time. Spike jitter was calculated to be variance of spike latencies of a neuron. 3 ms spike probability of a neuron was calculated as (total spike count within 3 ms) divided by (total spike count within the unitary stimulation interval).

Temporal discrimination and temporal resolution of two inputs converging onto a single VB TC neuron

To distinctly modulate different fibers separately, we utilized fine theta glass-driven electrical stimulation. Two theta glasses were located to separately activate two fibers in lemniscus. The pore size of the theta glass was about 1~3 μm, which can stimulate narrow

Please cite this article in press as: Kwak et al., Astrocytes Control Sensory Acuity via Tonic Inhibition in the Thalamus, Neuron (2020), https://doi.org/10.1016/j.neuron.2020.08.013

field. To verify that the fibers are separately modulated, we performed further experiments only when linear EPSC summation and no heterosynaptic short-term depression were found in recording VB TC neuron by simultaneous and paired-pulse stimulation of two theta electrodes, respectively. The intensity of stimulation was adjusted to a minimal value with about 50% failure rate by single stimulation (I_{50}), in order to recruit a minimal number of fibers. The probability of successful generation of spike pairs upon ten stimuli pairs was measured. The probability was calculated only when the first spike was successfully generated. If second stimulation fails to generate second action potential, only the intensity of second stimulation was adjusted to generates action potential up to three-fold of I_{50} ($3I_{50}$). Temporal resolution is defined as the inverse value of minimum time interval between the two stimuli, during which the postsynaptic TC neuron can discriminate the two inputs by successful firing (when the successful train rate is larger than 0%)

Population synchrony analysis

First, to analyze the degree of synchrony, the normalized cross-correlogram was obtained by dividing raw spike cross-correlogram by square-root (N_i^2+N_j^2), where N_i and N_j are the spike count of cross-correlation pair. The area under normalized cross-correlogram within the given synchrony window (red box, in this case ± 7.5 ms) was defined to be the degree of synchrony of neuronal pair (synchrony between Neuron-x and Neuron-y = $Synch_{x-y}$). To avoid redundancy and auto-correlation, mean $Synch_{x-y}$ was calculated only when x > y.

Novel object recognition test (NORT)

Habituation (Open field test)

Before NORT, mice were subjected to the habituation session for two consecutive days. In each day, a mouse was placed into an empty white-colored acrylic chamber (40 cm x 40 cm x 40 cm) and allowed to freely explore the chamber for 10 minutes. Distance traveled of the second day of habituation were analyzed as an indicator of locomotor activity (locomotion) using Ethovision XT software (Noldus).

Tactile NORT (tNORT)

After two consecutive days of habituation, NORT was performed in the same chamber used for open field test. Three types of cubes covered by sandpapers with various grits were used for the twostep tactile NORT (tNORT) (400-, 220- and 80-grit cubes, 3 cm x 3 cm x 5 cm). The objects were located at the positions with equal distance from the center of the chamber and from the walls of the chamber. First, at the learning phase, a mouse was exposed and allowed to freely explore two identical 400-grit cubes for 5 minutes. After 5 minutes of retention period in a separate cage, the mouse was re-exposed to the same chamber with one 400-grit cube replaced with 220-grit cube and allowed to explore the cubes for 5 minutes (Test (A) in Figure 7). The retention period and test session were iterated once again with the 220-grit cube replaced with 80-grit cube (Test (B) in Figure 7).

Standard NORT (NORT)

One day after the tNORT, mouse was subjected to the standard NORT (NORT). The sequence of NORT was same as tNORT except the objects. In NORT, we used two types of objects with different color and shape but similar volume. First, at the learning phase, a mouse was allowed to explore two identical objects for 5 minutes. After 5 minutes of retention, the mouse was placed back into the same chamber with one object replaced and allowed to freely explore the two objects for 5 minutes (Test (C) in Figure 7). The discrimination index of standard NORT was used as an indicator of short-term memory.

All the habituation, training and test sessions were performed in 40 lux light. In learning and test sessions, the time exploring each object was analyzed using Ethovision XT software (Noldus). The time that each mouse spent directing the nose toward the object with a distance of less than 1.5 cm or physically touching the nose to the objects was measured. The location of the novel object was counter-balanced among mice. Mice that did not explore the objects during learning phase, explored only one of the two objects during testing phase, or did not explore the two objects for at least 2 s were not included in this study. During every retention period, the chamber and cubes were cleaned with 70% ethanol and distilled water to remove any olfactory cues.

Cannula injection

Mice were anesthetized by intraperitoneal injection of 2% Avertin solution and fixed onto stereotaxic device. Mice were implanted with guide cannula (Plastics One) placed bilaterally into the VB thalamus (1.8 mm posterior relative to the bregma, 1.5 mm lateral relative to the midline and 3.0 mm below the brain surface). After the surgery, the mice were allowed at least 10 days for recovery. THIP (30 μM) was dissolved in aCSF contained (mM): 147 NaCl, 2.7 KCl, 1.2 $CaCl_2$ and 0.85 $MgCl_2$. The aCSF or THIP-containing aCSF is infused (0.1 μl/min, 0.2 μl) through injection cannula. The injection cannula was kept in place for 3 min after the end of the injection. By histologic confirmation, the data from improperly implanted mice were excluded.

Calculation of THIP concentration for THIP infusion *in vivo*

To calculate the concentration of THIP after infusion into VB thalamus *in vivo*, we first derived the diffusion coefficient of THIP in free medium. Given that there is no available diffusion coefficient of THIP in free medium, we utilized the SEGWE (Stokes–Einstein Gierer-Wirtz Estimation) (Evans et al., 2013, 2018) and derived the diffusion coefficient of THIP in free medium to be $1.036x10^{-9}$ m^2/s. Second, when molecules are diffusing through the extracellular matrix, geometric tortuosity and viscosity should be considered . With the

Please cite this article in press as: Kwak et al., Astrocytes Control Sensory Acuity via Tonic Inhibition in the Thalamus, Neuron (2020), https://doi.org/10.1016/j.neuron.2020.08.013

assumption of consideration of brain tissue as a porous medium and isotropic, the Fick's law ($D_{free} = kT/6\eta\pi R$) is adjusted by the tortuosity factor (λ) to $D = D_{free}(1/\lambda)^2$. Using experimental data that measured λ as 1.77 in the presence of 2% of 40kDA-macromolecule as a reference, apparent diffusion coefficient (D) of THIP is calculated to be 3.30×10^{-10} m^2/s.

QUANTIFICATION AND STATISTICAL ANALYSIS

All analysis were done blindly. The number of experimental samples, mean and SEM values are listed in Table S1. The numbers and individual dots refer to the number of cells unless otherwise clarified in figure legends. For data presentation and statistical analysis, Graphpad Prism (GraphPad Software) was used. For electrophysiology, Minianalysis (synaptosoft) and Clampfit (Molecular Devices) were used. For behavioral analysis, Ethovision XT (Noldus) was used. For image analysis, Imagej software was used. Statistical significance was set at $^*p < 0.05$, $^{**}p < 0.01$, $^{***}p < 0.001$, $^{****}p < 0.0001$. Data are presented as mean ± SEM.

Neuron, Volume *108*

Supplemental Information

Astrocytes Control Sensory Acuity via Tonic Inhibition in the Thalamus

Hankyul Kwak, Wuhyun Koh, Sangwoo Kim, Kiyeong Song, Jeong-Im Shin, Jung Moo Lee, Elliot H. Lee, Jin Young Bae, Go Eun Ha, Ju-Eun Oh, Yongmin Mason Park, Sunpil Kim, Jiesi Feng, Seung Eun Lee, Ji Won Choi, Ki Hun Kim, Yoo Sung Kim, Junsung Woo, Dongsu Lee, Taehwang Son, Soon Woo Kwon, Ki Duk Park, Bo-Eun Yoon, Jaeick Lee, Yulong Li, Hyunbeom Lee, Yong Chul Bae, C. Justin Lee, and Eunji Cheong

SUPPLEMENTAL FIGURES

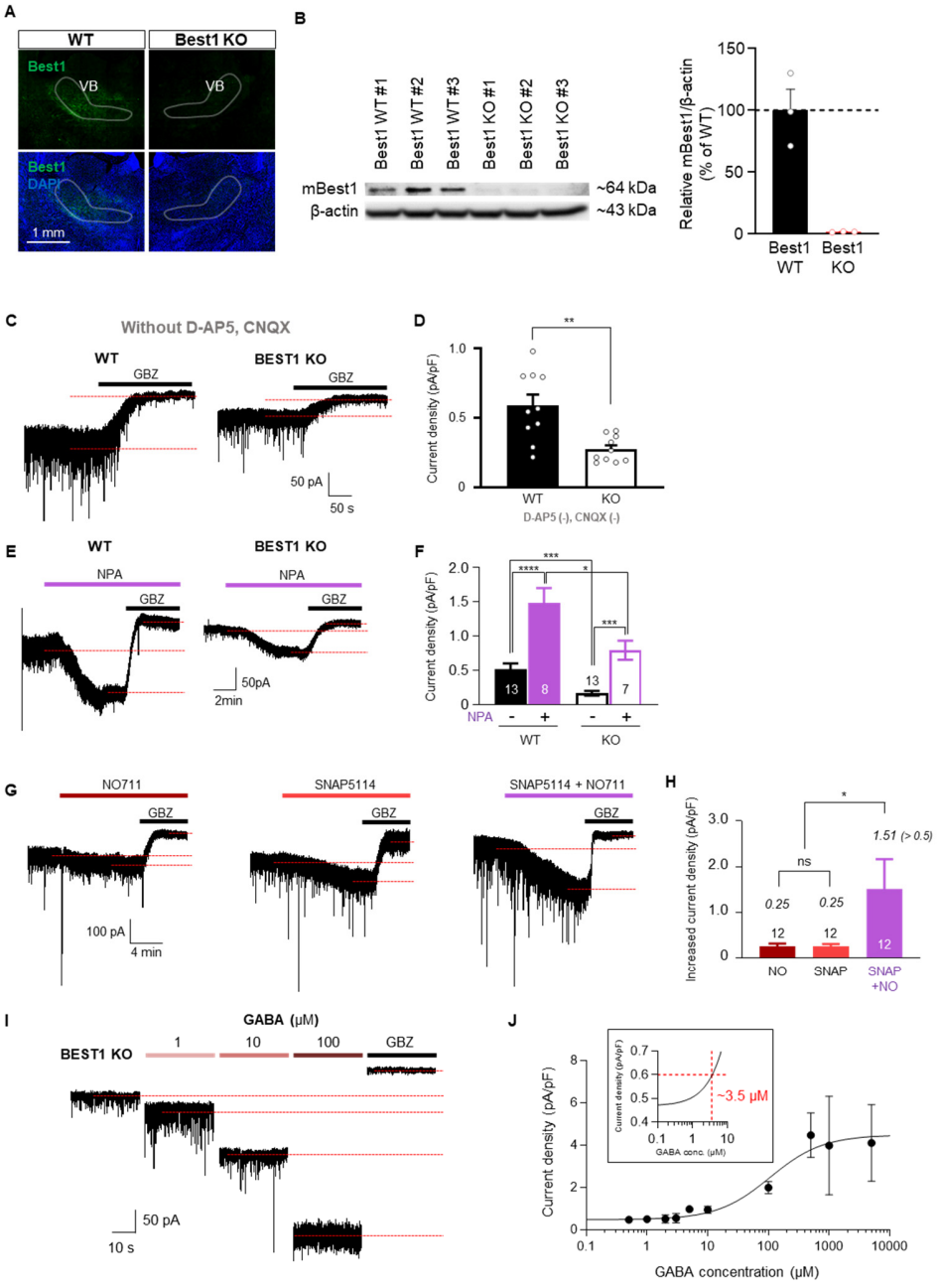

Figure S1. Properties of neurons from WT or Best1 KO mice. Related to Figure 1

(A) Representative immunohistochemistry image of Best1 in VB of WT or Best1 KO mice. (B) Western blot image (left) and bar-graph (right) of Best1 expression from thalamic samples of WT or Best1 KO mice (WT: N=3, 100±17.01, KO: N=3, 1.548±0.176). N indicates animal number. (C) Representative traces of GBZ-sensitive tonic current either from WT or Best1 KO mice in the absence of ionotropic glutamate receptor blockers. (D) Quantification of GBZ-sensitive tonic GABA currents from each group (WT: N=3/n=10, 0.5893± 0.0786, KO: N=3/n=10, 0.2747± 0.0294) (E-H) GATs

uptake extracellular GABA to reduce tonic current. (E) Representative traces of tonic GABA currents with application of nipecotic acide (NPA), a non-specific GATs blocker. (F) Quantification of GBZ-sensitive tonic GABA currents from each group. (WT: N=7/n=13, 0.5139±0.0871, WT-NPA: N=6/n=8, 1.488±0.212, KO: N=9/n=13, 0.1629±0.0353, KO-NPA: N=5/n=7, 0.7916±0.140) (G) Representative traces of tonic GABA currents with application of NO711 (10 μM) and/or SNAP5114 (100 μM) which are GAT1 and GAT3 blockers, respectively. (H) Quantification of GBZ-sensitive tonic GABA currents from each group. (NO711: N=6/n=12, 0.2511±0.0575, SNAP5114: N=6/n=12, 0.2494±0.0487, NO711+SNAP5114: N=4/n=12, 1.508±0.6522) We found that the inhibition of GAT1, GAT3, or both induced increase of tonic GABA, indicating that GATs are actively clearing up ambient GABA from exterior to interior of the cells (G,H). There was an increase of tonic GABA current by application of either NO711 or SNAP5114, showing that both GAT1 and GAT3 clear ambient tonic GABA to reduce tonic GABA current. Furthermore, the co-treatment of SNAP5114 and NO711 induced a larger tonic GABA current than sum of increment (Δcurrent) by each blocker indicating that the GABA transporters work cross-complementarily. Additionally, while the increase of tonic GABA current by NPA in Best1 KO was lower than that in WT, the effect of NPA in relative terms from basal was similar (i.e. three-fold of basal), showing that GATs' intrinsic transporting activity is independent of Best1 KO. (I) Representative trace of tonic current induced by various GABA concentrations from a TC neuron of Best1 KO mouse. (J) GABA-response curve of Best1 KO mice. Inset: calculation of basal GABA concentration. Calculated GABA concentration was about 3.5 μM. Data are represented as mean ± SEM. All the numbers in the figure refer to number of cells unless otherwise clarified.

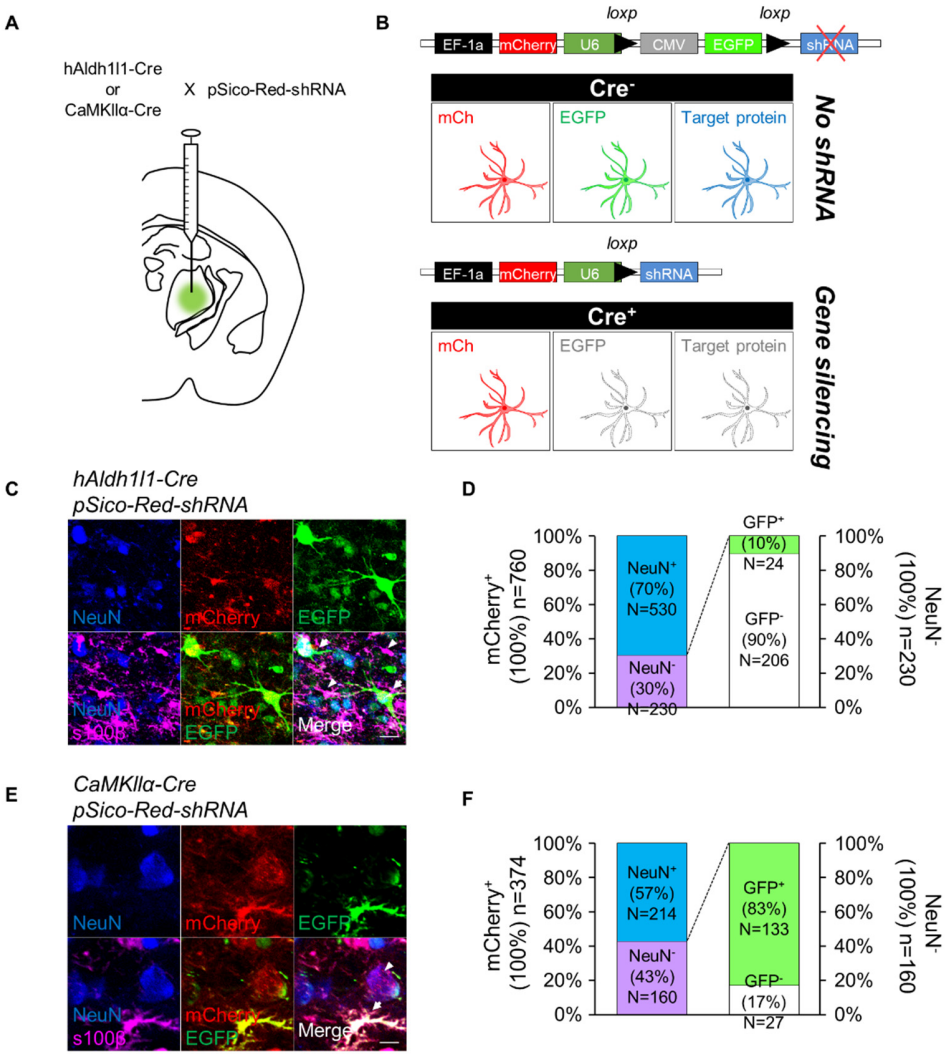

Figure S2. Experimental strategy and cell-type specificity of pSico-Red virus. Related to Figures 1, 2, 5, 6, 7

(A) Schematic of virus dual injection to ventrobasal (VB) nucleus of thalamus. Detailed injection protocol is in materials and method section. (B) Schematic of construction and fluorescent protein expression of pSico-Red-infected cells. The general construction strategy for pSico-Red is described in a previous publication (Jung et al., 2016). Without Cre recombinase (Cre^-), infected cells express both mCherry and EGFP, while stop codon hinder the expression of shRNA. In the presence of Cre recombinase (Cre^+), excision of EGFP and the stop codon between loxP sites leads to expression of shRNA. Together, we can visually identify gene-silencing by absence of EGFP signal in mCherry-expressing cells. (C) Representative confocal images of VB cells injected with hAldh1l1-Cre and pSico-Red-shDAO viruses. Arrows indicate Cre-negative cells which express both mCherry and EGFP. Arrowheads indicate Cre-positive cells with only mCherry signal. Note that mCherry(+)/EGFP(+) cells are NeuN-positive while mCherry(+)/EGFP(-) cells are co-localized with s100β which is a marker protein of astrocytes. Scale bar, 20μm. (D) Quantification of cell population. Among the mCherry-positive cells, few of NeuN-negative cells were GFP-positive. (E) Representative confocal images of VB cells injected with CaMKIIa-Cre and pSico-Red-shDAO viruses. Arrow indicates Cre-negative cells which express both mCherry and EGFP. Arrowhead indicates Cre-positive cells with only mCherry signal. Note

that mCherry(+)/EGFP(+) cells are s100β-positive while mCherry(+)/EGFP(-) cells are co-localized with NeuN. Scale bar, 10μm. (F) Quantification of cell population. Among the mCherry-positive cells, few of NeuN-negative cells were GFP-negative. This result shows that gene-silencing is performed in Cre-specific manner. All the numbers in the figure refer to number of cells unless otherwise clarified.

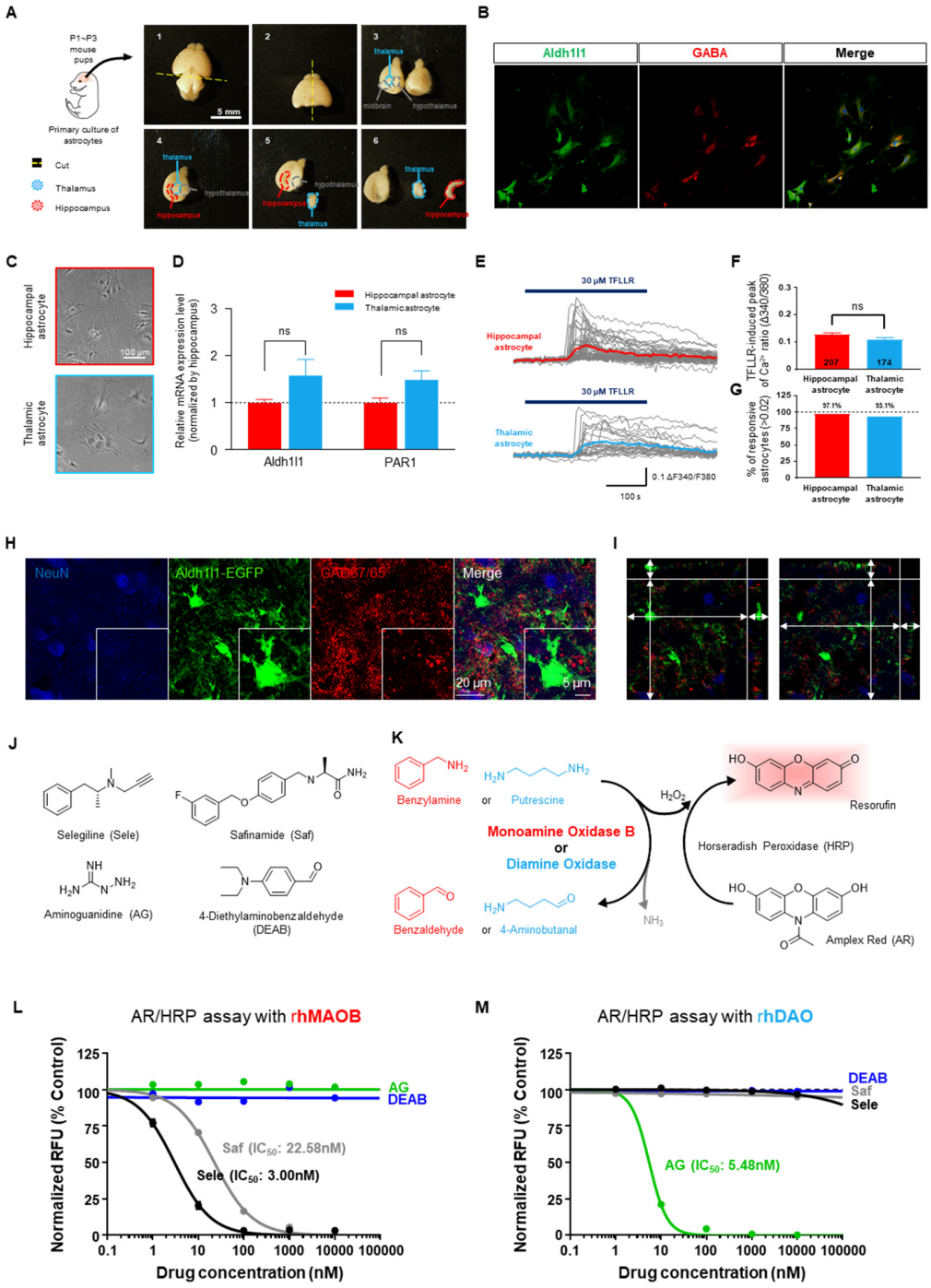

Figure S3. Primary culture of thalamic astrocyte and its characterization compared to primary hippocampal astrocyte. Immunostaining of GAD67/65. Cross-inhibition test with DAO, MAO-B and Aldh inhibitors. Related to Figures 1 and 2

(A) Dissection of thalamus (blue) and hippocampus (red) from the brain of P1~3 pups. (B) Immunocytochemistry images of thalamic astrocytes. Green: Aldh1l1 staining; Red: GABA staining. (C) Images of hippocampal and thalamic

astrocytes. (D) Relative mRNA expression of Aldh1l1 and PAR1 gene in thalamic astrocytes, compared to hippocampal astrocytes. (Hippo-Aldh1l1: N=4, 1.0±0.068, Thal-Aldh1l1: N=4, 1.571±0.346, Hippo-PAR1: N=4, 1.0±0.101, Thal-PAR1: N=4, 1.479±0.197) (E) Representative Ca^{2+} responses by TFLLR application, and the averaged response (colored bold trace) in hippocampal and thalamic astrocytes. (F) Averaged peak of Ca^{2+} responses by TFLLR application in hippocampal and thalamic astrocytes. (Hippo: n=207, 0.1272±0.0065, Thal: n=174, 0.1103±0.0063) (G) The percentage of TFLLR-responsive cells in hippocampal and thalamic astrocytes. (H) Immunostaining images of GAD67/65 in Aldh1l1-EGFP mouse. Confocal images show that GAD67/65 is absent in both NeuN-positive and EGFP-positive area. Certain number of GAD-positive dots seem to be localized in GABAergic axon terminals from thalamic reticular nucleus (TRN). (I) Z-stack analysis also shows no co-localization of GAD with either NeuN or EGFP. (J) Structures of selegiline (irreversible MAO-B inhibitor), safinamide (reversible MAO-B inhibitor), aminoguanidine (reversible DAO inhibitor) and 4-Diethylaminobenzaldehyde (reversible Aldh family inhibitor). (K) Principle of AR/HRP assay for MAO-B or DAO enzyme activity assay. (L) Dose-response curve of the inhibitors on rhMAOB enzyme activity. (M) Dose-response curve of the inhibitors on rhDAO enzyme activity. Data are represented as mean ± SEM. All the numbers in the figure refer to number of cells unless otherwise clarified.

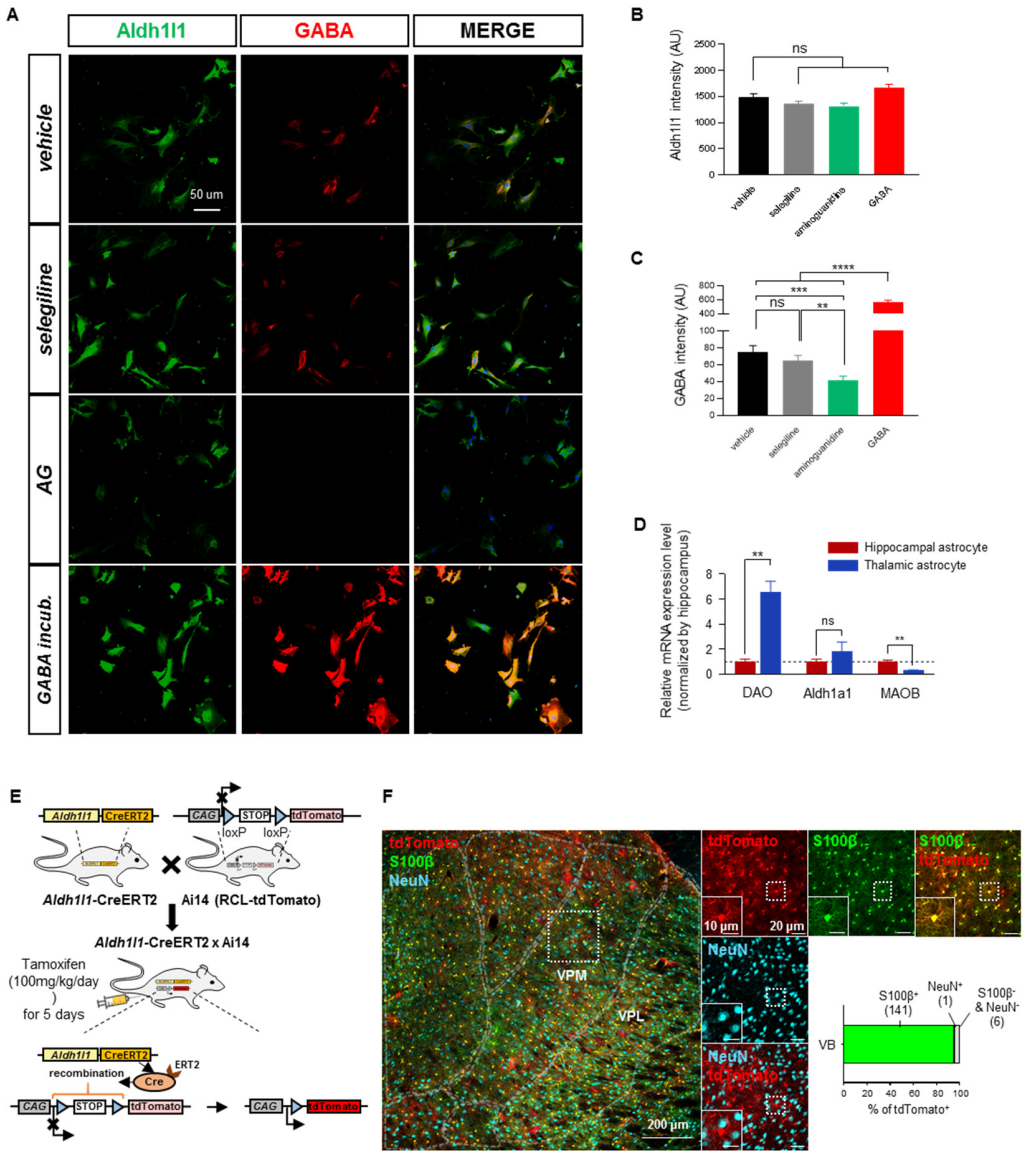

Figure S4. DAO-dependent GABA synthesis of thalamic astrocyte. Generation of Aldh1l1-CreERT2 x RCL-tdTomato mouse. Related to Figure 3

(A) Representative immunocytochemistry images in each condition. Green: Aldh1l1 staining; Red: GABA staining. (B) Summary of Aldh1l1 intensity from each condition. (vehicle: n=135, 1484±70.72, selegiline: n=186, 1355±59.60, aminoguanidine: n=168, 1310±53.87, GABA incubation: n=190, 1664±62.67) (C) Summary of GABA intensity from each condition. (vehicle: n=135, 65.04±7.643, selegiline: n=186, 64.72±6.124, aminoguanidine: n=167, 41.37±4.936, GABA incubation: n=190, 561.1±31.09) (D) Relative mRNA expression of DAO, Aldh1a1 and MAOB gene in thalamic astrocytes, compared to hippocampal astrocytes. (E) Aldh1l1-CreERT2 mouse was crossed with reporter line, Ai14 (RCL-tdTomato) mouse. To activate CreERT2, tamoxifen (100mg/kg/day) was administered with intraperitoneal

injection for five days. (F) Immunohistochemistry images in thalamic VB. Inset: Quantification of tdTomato+ population with S100β+, NeuN+ and S100β-/NeuN- cells in thalamic VB area. Data are represented as mean ± SEM. All the numbers in the figure refer to number of cells unless otherwise clarified.

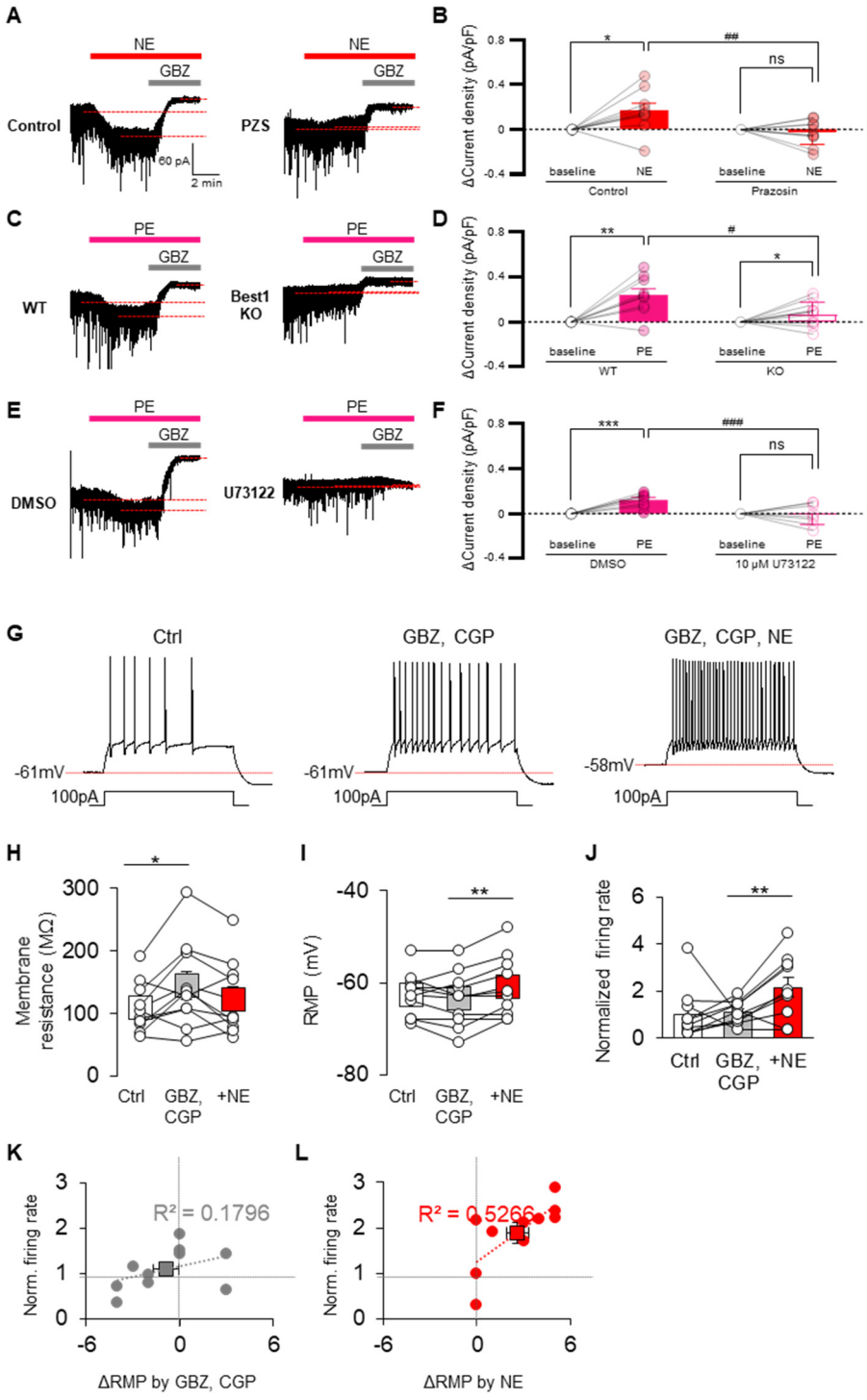

Figure S5. Signaling pathway of NE-dependent tonic current release from thalamic astrocytes and GABA-independent NE effects on thalamic neurons. Related to Figure 4

(A-F) Signaling pathway of NE-dependent tonic GABA increase. (A) Representative traces of NE-dependent tonic current increase with or without prazosin (PZS) (B) Bar-graph of NE-dependent tonic current increase. (C) Representative traces of PE-dependent tonic current increase in WT or KO mice. (NE: N=7/n=9, 0.1707±0.0642, PZS-NE: N=3/n=10, -0.0264±0.035) (D) Bar-graph of PE-dependent tonic current increase. (PE: N=5/n=9,

0.2395±0.0567, KO-PE: N=5/n=12, 0.0687±0.0306) (E) Representative traces of PE-dependent tonic current increase with or without U73122, a selective PLC inhibitor. (F) Bar-graph of PE-dependent tonic current increase with or without PLC blockade. (DMSO: N=2/n=8, 0.1203± 0.0219, U73122: N=2/n=8, -0.00636±0.0325) (A,B) NE-induced increase of tonic GABA was blocked by 10 μM prazosin (PZS), a selective inhibitor of α1-adrenoreceptor. (C,D) Application of 10 μM phenylephrine (PE), a selective agonist of α1-adrenoreceptor, mimicked the NE-induced increase of tonic GABA. (E,F) The tonic GABA increase by PE was abolished by pre-incubation of PLC inhibition, indicating that NE-dependent release of tonic GABA is mainly via α1-adrenoreceptor-PLC signaling pathway. (G) Representative traces of spike generation induced by 100 pA-current injection in the presence or absence of GBZ, CGP55845, a GABAB receptor selective antagonist and NE. Note that in the presence of GBZ and CGP, application of NE depolarizes the resting membrane potential (RMP) and firing rate. (H) Bar-graph of membrane resistance. (I) Bar-graph of RMP. (J) Bar-graph of normalized firing rate. (K,L) Correlation of ΔRMP and normalized firing rate. Data are represented as mean ± SEM. All the numbers in the figure refer to number of cells unless otherwise clarified.

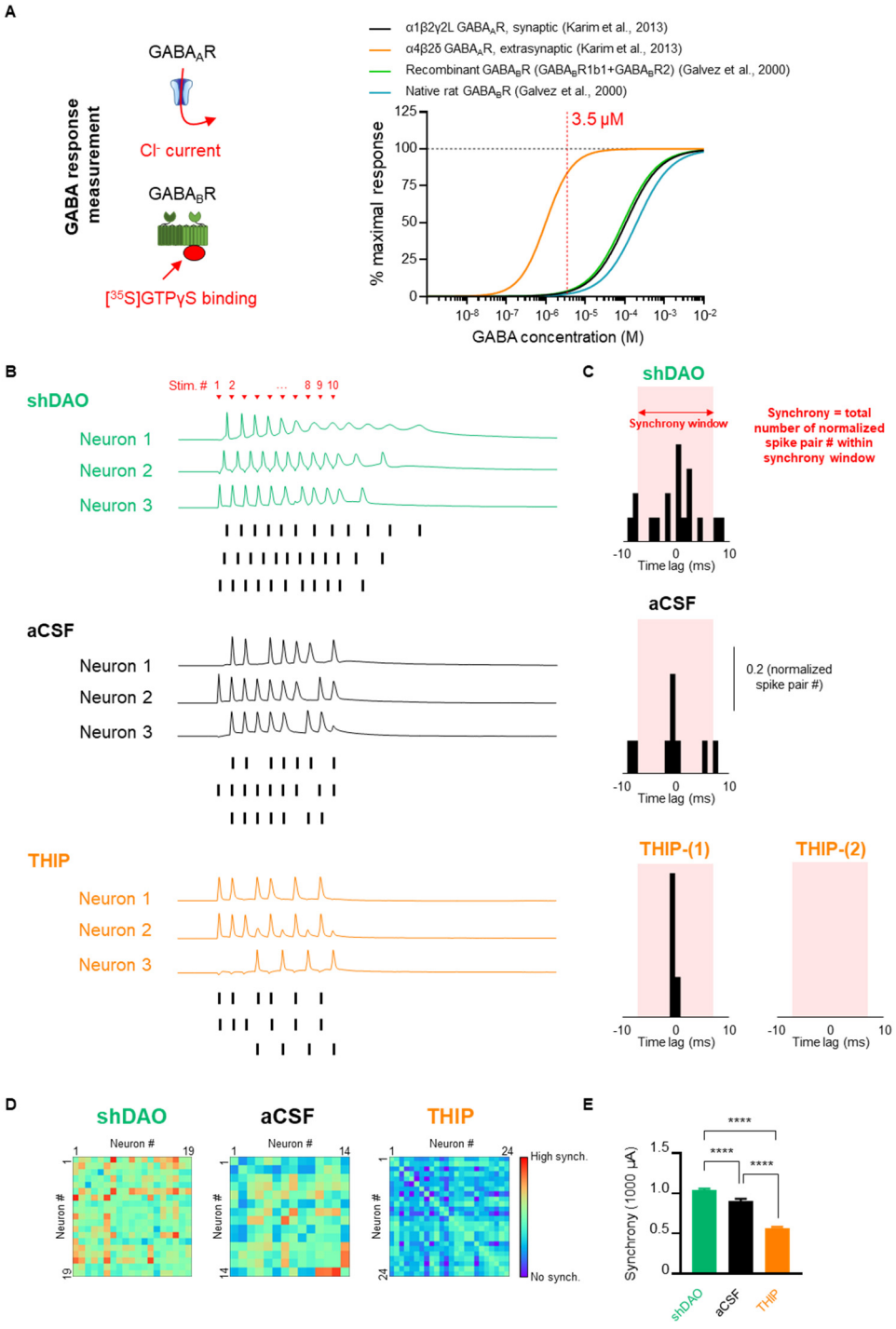

Figure S6. Effect of tonic GABA on the population synchrony. Related to Figure 5

(A) Schematic illustration (left) and dose-response curve (right) of the GABA receptors expressed in thalamic neurons based on previous reports. (B) Three representative traces and spike timings from each group. Note that neuron 2 and neuron 3 of THIP group have no synchronized spike at all, because of occasional failure of spike generation. (C) Representative cross-correlogram from each group. The normalized cross-correlogram was obtained by dividing the spike cross-correlogram by square-root (N_1^2+N_2^2), where N_1 and N_2 are the spike count of cross-correlation pair. There are more spikes within -7.5 to +7.5 ms in low tonic GABA condition (shDAO). In

contrast, in THIP group, some pairs show a synchronous firing with very small jitter (THIP-1) whereas other pairs did not show any synchrony at all (THIP-2). This type of pair with no spike pair within 10 ms window has never been observed in aCSF and shDAO group. (D) Synchrony matrices of individual neuronal pairs. (E) Bar-graph of synchrony. (shDAO: n=171, 1.041±0.0193, aCSF: n=91, 0.902±0.0309, THIP: n=276, 0.57±0.0132) n indicates spike pair count. To quantitatively show whether tonic GABA increases synchronization regardless the total number of spikes, we adopted cross-correlogram-based analysis of synchronization as previously described . Briefly, the area under cross-correlogram between the given synchrony window (red box, in this case ±7.5 ms). We found that the synchrony is lower in high tonic $GABA_AR$ conductance group (THIP). In summary, we observed that under THIP condition synaptic pair's synchrony is enhanced in some pairs but not in others, whereas under shDAO condition overall synchrony among multiple pairs was enhanced, implying that tonic GABA increases the acuity by enhancing temporal fidelity in some pairs while filtering out the signal transmission in other pairs. Data are represented as mean ± SEM.

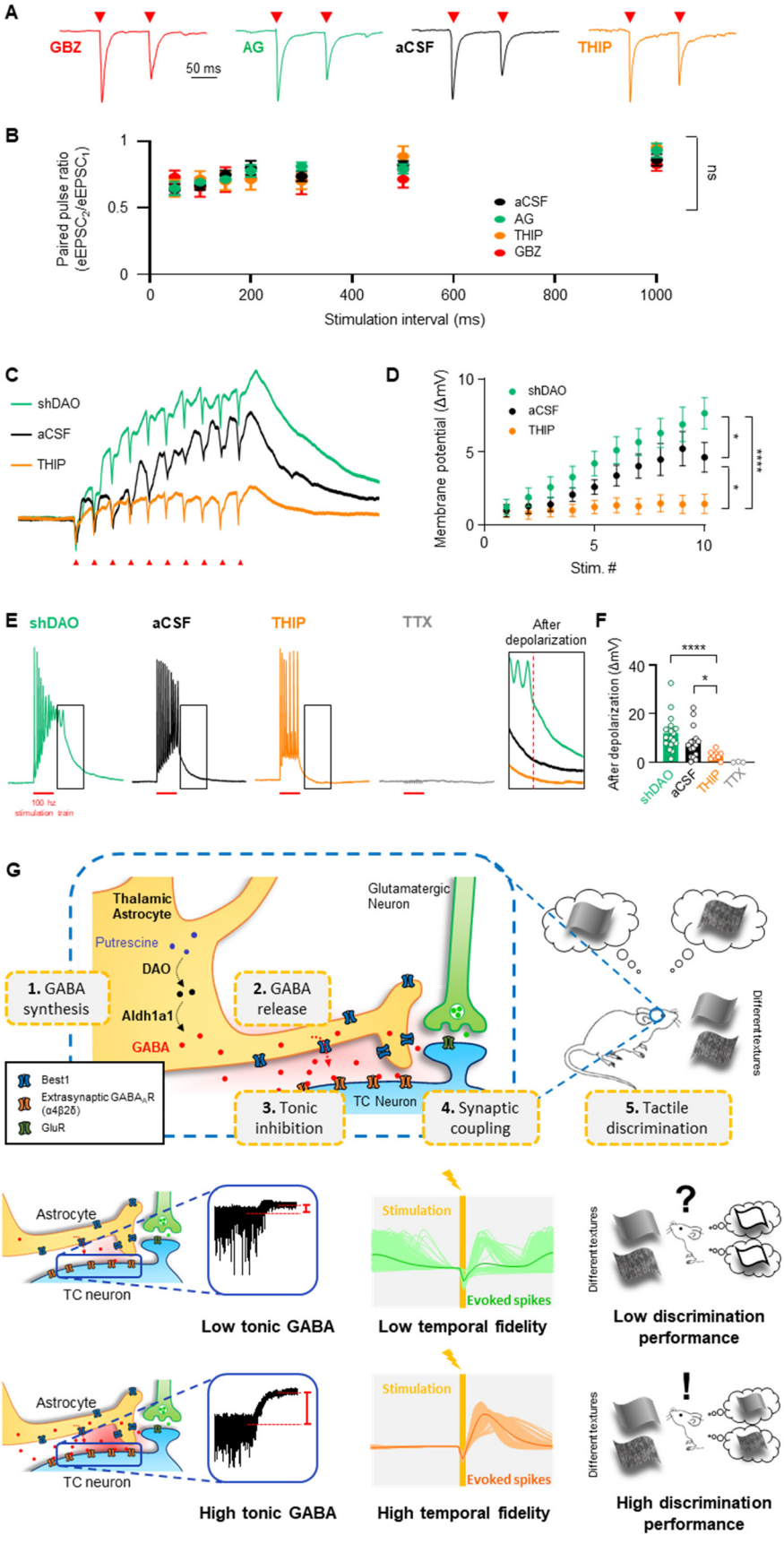

Figure S7. Synaptically-elicited responses of TC neurons. Related to Figures 5 and 7

(A) Representative traces of EPSCs evoked by lemniscal paired-pulse stimulation with 100 ms inter-stimul us-interval. (B) Summary graph of paired-pulse ratio by various intervals. (C) Representative traces of dep olarizing membrane potential by 100 Hz stimulation train with 200 μA intensity. (D) Quantification of mem brane potential at varying stimuli numbers. (E) Representative traces of spikes and after depolarization du ring and after 100 Hz stimulation. Inset: Representative traces of after depolarization. Levels of after depo larization were analyzed at 0.17s after the start of stimulation train. The analysis point is indicated with a red dashed line. (F) Bar-graph of after depolarization. (shDAO: n=18, 12.09±1.687, aCSF: n=16, 7.956±1.5 96, THIP: n=12, 2.454±0.5143, TTX: n=3, 0.0833±0.1286) (G) Schematic working model of tonic GABA in thalamus. Data are represented as mean ± SEM. All the numbers in the figure refer to number of cells u nless otherwise clarified.